

Article

The CYGNO Experiment

Fernando Domingues Amaro¹, Elisabetta Baracchini^{2,3}, Luigi Benussi⁴, Stefano Bianco⁴, Cesidio Capoccia⁴, Michele Caponero^{4,5}, Gianluca Cavoto^{6,7}, André Cortez^{2,3}, Igor Abritta Costa⁸, Emiliano Dané⁴, Giorgio Dho^{2,3}, Emanuele Di Marco⁶, Giulia D’Imperio⁶, Flaminia Di Giambattista^{2,3}, Robert Renz Marcelo Gregorio⁹, Francesco Iacoangeli⁶, Herman Pessoa Lima Júnior¹⁰, Amaro da Silva Lopes Júnior⁸, Giovanni Maccarrone⁴, Rui Daniel Passos Mano¹, Michela Marafini¹¹, Giovanni Mazzitelli⁴, Alasdair McLean⁹, Andrea Messina^{6,7}, Cristina Maria Bernardes Monteiro¹, Rafael Antunes Nobrega⁸, Igor Fonseca Pains⁸, Emiliano Paoletti⁴, Luciano Passamonti⁴, Sandro Pelosi⁶, Fabrizio Petrucci^{12,13}, Stefano Piacentini^{6,7}, Davide Piccolo⁴, Daniele Pierluigi⁴, Davide Pinci^{6*}, Atul Prajapati^{2,3}, Francesco Renga⁶, Rita Joana da Cruz Roque¹, Filippo Rosatelli⁴, Andrea Russo⁴, Joaquim Marques Ferreira dos Santos¹, Giovanna Saviano^{4,14}, Neil Spooner⁹, Roberto Tesauro⁴, Sandro Tomassini⁴ and Samuele Torelli^{2,3}.

¹ LIBPhys, Department of Physics, University of Coimbra, 3004-516 Coimbra, Portugal; famaro@uc.pt (F.D.A.); cristinam@uc.pt (C.M.B.M.); ritaroque@fis.uc.pt (R.J.d.C.R.); RDPMano@uc.pt (R.D.P.M.); jmf@uc.pt (J.M.F.d.S.)

² Gran Sasso Science Institute, 67100, L’Aquila, Italy; andre.f.cortez@gmail.com (A.C.); giorgio.dho@gssi.it (G.D.); flaminia.digiambattista@gssi.it (F.D.G.); atul.prajapati@gssi.it (A.P.); samuele.torelli@gssi.it (S.T.)

³ Istituto Nazionale di Fisica Nucleare, Laboratori Nazionali del Gran Sasso, 67100, Assergi, Italy

⁴ Istituto Nazionale di Fisica Nucleare, Laboratori Nazionali di Frascati, 00044, Frascati, Italy; luigi.benussi@lnf.infn.it (L.B.); stefano.bianco@lnf.infn.it (S.B.); Cesidio.Capoccia@lnf.infn.it (C.C.); caponero@frascati.enea.it (M.C.); Emiliano.Dane@lnf.infn.it (E.D.); giovanni.maccarrone@lnf.infn.it (G.M.); giovanni.mazzitelli@lnf.infn.it (G.M.); Emiliano.Paoletti@lnf.infn.it (E.P.); luciano.passamonti@lnf.infn.it (L.P.); Davide.Piccolo@lnf.infn.it (D.P.); Daniele.Pierluigi@lnf.infn.it (D.P.); filippo.rosatelli@lnf.infn.it (F.R.); arusso@lnf.infn.it (R.T.); sandro.tomassini@lnf.infn.it (S.T.)

⁵ ENEA Centro Ricerche Frascati, 00044, Frascati, Italy

⁶ Istituto Nazionale di Fisica Nucleare, Sezione di Roma, 00185, Rome, Italy; gianluca.cavoto@roma1.infn.it (G.C.); emanuele.dimarco@roma1.infn.it (E.D.M.); giulia.dimperio@roma1.infn.it (G.D.); francesco.iacoangeli@roma1.infn.it (F.I.); andrea.messina@uniroma1.it (A.M.); Alessandro.Pelosi@roma1.infn.it (S.P.); stefano.piacentini@uniroma1.it (S.P.); davide.pinci@roma1.infn.it (D.P.); francesco.renga@roma1.infn.it (F.R.)

⁷ Dipartimento di Fisica, Università La Sapienza di Roma, 00185, Roma, Italy

⁸ Universidade Federal de Juiz de Fora, Faculdade de Engenharia, 36036-900, Juiz de Fora, MG, Brasil; igorabritta@gmail.com (I.A.C.); rafael.nobre@ufjf.edu.br (R.A.N.);igor.pains@ufjf.edu.br (I.P.); silva.lopes@ufjf.edu.br (A.D.S.L.J.)

⁹ Department of Physics and Astronomy, University of Sheffield, Sheffield, S3 7RH, UK; robert.gregorio@sheffield.ac.uk (R.R.M.G.); ali.mclean@sheffield.ac.uk (A.C.M.L.); n.spooner@sheffield.ac.uk (N.S.)

¹⁰ Centro Brasileiro de Pesquisas Físicas, Rio de Janeiro 22290-180, RJ, Brazil; hlima@cbpf.br

¹¹ Museo Storico della Fisica e Centro Studi e Ricerche “Enrico Fermi”, Piazza del Viminale 1, 00184, Roma, Italy; Michela.Marafini@roma1.infn.it

¹² Dipartimento di Matematica e Fisica, Università Roma TRE, 00146, Roma, Italy; fabrizio.petrucci@uniroma3.it

¹³ Istituto Nazionale di Fisica Nucleare, Sezione di Roma TRE, 00146, Roma, Italy

¹⁴ Dipartimento di Ingegneria Chimica, Materiali e Ambiente, Sapienza Università di Roma, 00185, Roma, Italy

* Correspondence: davide.pinci@roma1.infn.it

Citation: Amaro, F.D.; Baracchini, E.; Benussi, L.; Bernardes Monteiro, C.M.; Bianco, S.; Capoccia, C.; Caponero, M.; Cavoto, G.; Cortez, A.; I. A. Costa; et al. The CYGNO Experiment. *Physics* **2021**, *1*, 1–30. <https://doi.org/>

Received:

Accepted:

Published:

Publisher’s Note: MDPI stays neutral with regard to jurisdictional claims in published maps and institutional affiliations.

Copyright: © 2021 by the authors. Submitted to *Physics* for possible open access publication under the terms and conditions of the Creative Commons Attribution (CC BY) license (<https://creativecommons.org/licenses/by/4.0/>).

Abstract: The search for a novel technology able to detect and reconstruct nuclear and electron recoil events with an energy of few keV has become more and more important as long as vast regions of high mass Dark Matter (DM) candidate have been excluded. Moreover, a detector sensitive to incoming particle direction will be crucial, in case of DM discovery, to open the possibility of study its properties and origin. Gaseous Time Projection Chambers (TPC) with optical readout are very promising detectors combining the detailed event information provided by the TPC technique to the high sensitivity and granularity of last generation scientific light

⁵ possibility of study its properties and origin. Gaseous Time Projection Chambers (TPC) with optical readout are very promising detectors combining the detailed event information provided by the TPC technique to the high sensitivity and granularity of last generation scientific light

sensors. The CYGNO experiment (a CYGNus module with Optical readout) aims at exploiting the optical readout approach of multiple-GEM structures in large volume TPC for the study of rare events as interactions of low mass DM or solar neutrinos. The combined use of high-granularity sCMOS camera and fast light sensors allows the reconstruction of the 3D direction of the tracks, offering good energy resolution and very high sensitivity in the few keV energy range, together with a very good particle identification useful to distinguish nuclear recoils from electronic recoils. This experiment is part of the CYGNUS proto-collaboration which aims at constructing a network of underground observatories for directional DM search. A 1 cubic meter demonstrator is expected to be built in 2022/23 aiming at a larger scale apparatus (30m^3 - 100 m^3), in a later stage.

Keywords: Dark Matter; Time Projection Chamber; Optical Readout

1. Introduction

The presence in the Universe of large amount of not-luminous matter (usually referred to as *Dark Matter (DM)*) is nowadays an established, yet still mysterious, paradigm [1]. Deciphering its essence is one of the most compelling tasks for fundamental physics today. Electrically neutral and very low interacting particles with a mass in the range between few to thousands of GeV are usually referred to as *Weakly Interacting Massive Particles (WIMPs)*. They represent a well motivated DM candidate, independently predicted by extension of the Standard Model of particle physics and the Λ -CDM model of cosmology. The measurements of the rotational curve of our Galaxy suggest the presence of a DM halo, through which the ordinary, luminous galactic matter is travelling in its revolution around the Galactic center. This creates a relative motion between an observer on Earth and the particles in the halo, that scientists seek to exploit to detect DM through their elastic scattering with ordinary matter. In particular, nuclear recoils are expected to be the clearest evidence of WIMP interactions.

Given their rarity, the main experimental challenge of direct DM searches in the GeV mass region is to discriminate the low energy nuclear recoils (1-100 keV) from interactions induced by other particles, which have largely higher rates. The apparent WIMP wind would create two peculiar effects for an observer on the Earth, that can be exploited for a positive identification of a DM signal. Since in its rotation around the Sun the Earth orbital velocity is anti-parallel to the DM wind during summer and parallel during winter, the observed DM rates inside the detector are expected to display a seasonal modulation of few percent. A much more robust signature is provided by the diurnal directional modulation of the DM signal. The peak flux, in fact, comes from the direction of solar motion around the center of our Galaxy, which happens to point towards the Cygnus constellation. Due to the Earth rotation around its axis (oriented at 48° with respect to the direction of the DM apparent wind), an observer on Earth would see the average DM incoming direction changing of $\sim 96^\circ$ every 12 sidereal hours. The amplitude of the modulation depends on the relative angle between the laboratory frame and the Earth axis, with the maximum at 45° inclination and no modulation along directions parallel to the axis.

The determination of the incoming direction of the WIMP can therefore provide a correlation with an astrophysical source [2] that no background can mimic. Directional measurements can furthermore discriminate between various DM halo models and provide constraints on WIMP properties, like no other non-directional detector [2].

While the last few decades have seen enormous advances in direct DM searches, leading to many orders of magnitude improvement for masses larger than 10 GeV, the O(GeV) mass range still remains theoretically well motivated [3? –5]. Despite the great effort devoted to lower the threshold for nuclear recoils to include DM scattering directly from electrons [6–11] or to exploit new signatures such as the Migdal effect [12–15] and photon bremsstrahlung [?], the O(GeV) mass range is still largely unexplored.

Given the kinematics of the elastic scattering, a direct DM detection experiment achieves its best sensitivity for WIMP masses equal to the target mass nuclei. The maximum fraction ϵ of the energy that can be transferred to a target of mass m_T by a WIMP of mass m_χ is in fact given by:

$$\epsilon = \frac{4\rho}{(\rho + 1)^2} \quad (1)$$

with $\rho = \frac{m_T}{m_\chi}$. Therefore, low mass target nuclei, such as hydrogen and helium, are the best choices to maximise the sensitivity to O(GeV) WIMP masses.

The CYGNO experiment proposes an innovative approach to the direct DM search challenge. A high resolution 3D gaseous Time Projection Chamber (TPC) operated at atmospheric pressure is employed with light target nuclei such as helium and fluorine, to boost the sensitivity to O(GeV) WIMP masses for both Spin Independent (SI) and Spin Dependent (SD) coupling. It is also important to notice that light target nuclei will result in longer track lengths, easing the determination of their direction and thus providing directional sensitivity. Studies to add a hydrogen based gas to provide even lighter targets are ongoing. The topological signature of the recoil event improves also particle identification and hence rejection of natural radioactivity backgrounds down to low energy thresholds. The possibility of operation at atmospheric pressure guarantees a reasonable volume to target mass ratio, while at the same time allowing to reduce the requirements on the vessel (hence internal backgrounds). The possibility of a high resolution 3D TPC, such as the one foreseen by this project, will allow CYGNO to explore new physics cases as, among the others, the elastic scattering of sub-GeV DM [16] and of solar neutrinos [17,18].

The results obtained with current prototypes (Sec. 3) are the basis for the design of a 1 m³ demonstrator (CYGNO PHASE_1), that is the subject of this paper. According to the performance of this, the collaboration will propose a larger detector for a competitive experiment (CYGNO PHASE_2). With this program, CYGNO fits in the context of the wider international CYGNUS effort, to establish a Galactic Directional Recoil Observatory that can test the DM hypothesis beyond the Neutrino Floor and measure the coherent scattering of neutrinos from the Sun and Supernovae [19].

2. The Experimental Approach

The CYGNO experiment goal is to deploy at Laboratori Nazionali del Gran Sasso a high resolution TPC with optical readout based on Gas Electron Multipliers (GEMs) working with a helium/fluorine gas mixture at atmospheric pressure for the study of rare events with energy releases in the range 1-100 keV.

Although challenging, gaseous TPCs constitute a promising approach to directional DM searches providing a set of crucial features:

- TPC are usually made by a sensitive volume, filled with gas or liquid, enclosed between an anode and a cathode generating a suitable electric field in it [20–22].
- The passage of a ionising particle produces free electrons and ions that start to drift towards the above mentioned electrodes. These are usually segmented and readout to provide a granular information about the charge collection point on the plane. The third coordinate can be evaluated from the drift time measurement. Therefore, TPC are inherently 3D detectors capable to acquire large sensitive volumes, with a lower amount of readout channels with respect to other high precision 3D tracking systems.
- Gaseous detectors can feature very low energy detection thresholds. In gas, a single electron cluster can be produced with energy releases of the order of few tens of eV and this has a very good chance of reaching the multiplication region and to produce a detectable signal.
- A measurement of the total ionisation indicates the energy released by the recoil and (depending on the readout plane granularity) the profile of the energy deposit along

the track can be measured with high precision, providing excellent background discrimination.

- 110 • The track itself indicates the axis of the recoil and the charge profile along it encodes the track orientation (*head-tail*), providing an additional powerful observable for DM searches.
- 115 • A large choice of gasses can be employed in TPC, including light nuclei with odd number of nucleons (as Fluorine), which are sensitive to both SI and SD interactions also in the O(GeV) mass region.
- 120 • A room-temperature and atmospheric-pressure detector results in operational and economical advantages, with no need for cooling or vacuum sealing. These choices allow for a much more compact experiment realization and straightforward scaling when compared to cryogenic solutions currently dominating the DM direct search scene.
- 125 • The use of a gaseous target reduces the interaction probability with respect to denser material (liquid or solid). Anyway, TPCs up to 100 m^3 of active volume have already been successfully operated [23,24] and up nearly 20000 m^3 approved for construction in the neutrino field [25], showing the feasibility of very large detectors with large active masses.

2.1. The Optical Readout

Gas luminescence is a well studied and established mechanism: charged particles traveling in the gas can ionize atoms and molecules but can also excite them. During the de-excitation processes, photons are emitted. The amount and spectrum of light produced strongly depends on the gas, on its density and the on the possible presence and strength of an electric fields [26–29].

The idea of detecting the light produced during the multiplication processes, proposed many years ago [30], has received in recent years a renewed attention. The optical readout approach, in fact, offers several advantages:

- 135 • highly performing optical sensors are being developed for commercial applications and can be easily procured;
- light sensors can be installed outside the sensitive volume reducing the interference with high voltage operation and the gas contamination;
- the use of suitable lenses allows to image large $O(1) \text{ m}^2$ areas with a single sensor while maintaining $O(100) \mu\text{m}$ effective pixels transverse size.

In recent years, an increasing number of tracking detectors have started employing Micro-Pattern Gaseous Detectors (MPGDs). Their major advantages are the very high achievable granularity and rate capability, together with mechanical robustness. The production technology for MPDG guarantees nowadays very high quality devices, providing stable and uniform operation. In particular GEMs [31] have already been used to equip very large areas with high space and time resolution [23], and have more recently been employed coupled to pixelised light sensors showing very good performances [26,32–34].

Charge Coupled Devices (CCD) have been widely used in the past as high granularity light sensors for optical TPC approaches [34–36]. CCDs main limitation for the study of rare events in the 1-100 keV energy range is represented by the high level of readout noise, up to 5 to 10 electrons rms per pixel. More recently, cameras based on the CMOS technology have been developed (sCMOS), that can reach tens of millions of pixels, with, sub-electron readout noise and single photon sensitivity.

The CYGNO collaboration proposed the introduction of sCMOS-based optical devices for GEM readout in 2015 [37]. The high sensitivity of this technique resulted in a very good performance in the particle detection not only at the energies of interest for DM searches (as is illustrated in Sec.3), but also for minimum ionising particle, from both cosmic rays and high energy electrons [33,38–41].

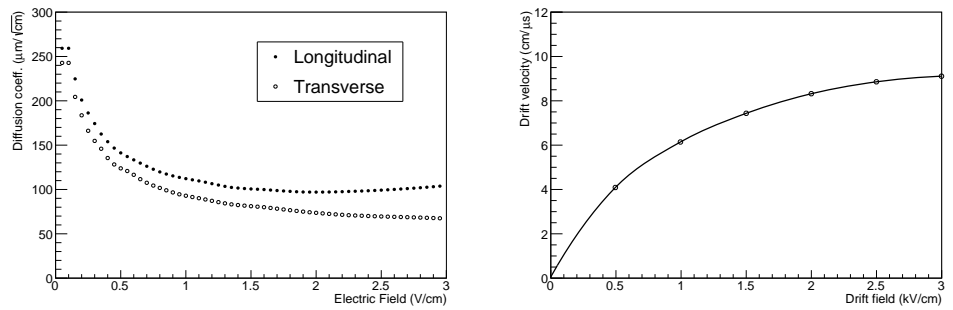


Figure 1. Transverse and longitudinal diffusion coefficients for He/CF₄ 60/40 (left) and electron drift velocity as a function of the drift field (right).

Because the current frame rate available for CCD or sCMOS is still low compared to the temporal extent of typical TPC signals, such devices can provide only 2D projection of the recoil track. In order to achieve 3D track reconstruction, the CYGNO experiment aims at complementing the sCMOS image information with the signal of a fast light sensors (PMT or SiPM), that can provide the track profile along the drift direction.

2.2. The Gas Mixture

The relative photon yield, defined as the ratio between the number of produced photons and the total number of secondary electrons produced in the avalanche process, and in general the overall detector performances, are significantly dependent on the gas characteristics: ionization statistics, transport properties (drift velocity and diffusion), electron multiplication and light production. In the context of optical TPCs for DM searches, CF₄ is a particularly interesting gas because of its well known properties as efficient scintillator, and the large fluorine content that provides sensitivity to spin-dependent WIMP-proton interactions. It was demonstrated by previous studies [26] that CF₄-based mixtures have electro-luminescence emission spectra with a large peak around 600 nm, where Si-based sensors (CCD or sCMOS) offer their highest quantum efficiency.

For these reasons, He/CF₄ mixtures in different proportions were extensively studied within the CYGNO project. The best performance were found for a mixture with 60% helium and 40% CF₄ [42,43]. The behaviors of the diffusion coefficients and drift velocity for different electric fields were calculated with Garfield [44,45] and are shown in Fig. 1.

An average energy loss per single ionization of 42 eV was estimated. As it can be seen from Fig. 1, a remarkable additional advantage of the use of CF₄ is the small electron diffusion, that can provide a reduced deterioration of the track original shape.

The effective ranges of electron and He-nuclei recoils were simulated respectively with the GEANT4 [46] and SRIM software¹. The average 3D ranges (i.e. the distance between production and absorption point) as a function of the particle kinetic energy are shown in Fig. 2:

- He-nuclei recoils have a sub-millimetre range up to energies of 100 keV and are thus expected to produce bright spots with sizes mainly dominated by diffusion effects;
- low energy (less than 10 keV) electron recoils are in general larger then He-nuclei recoils with same energy and are expected produce less intense spot-like signals. For a kinetic energy of 10 keV, the electron range becomes longer than 1 mm and for few tens of keV, tracks of few centimetres are expected.

¹ Visit the <http://www.srim.org/> site for more information

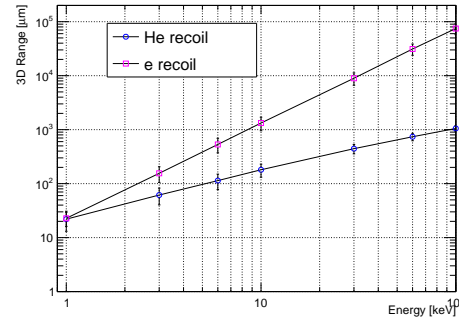


Figure 2. Average 3D distance between production and absorption point for electron- and He-nucleus recoils as a function of their kinetic energy.

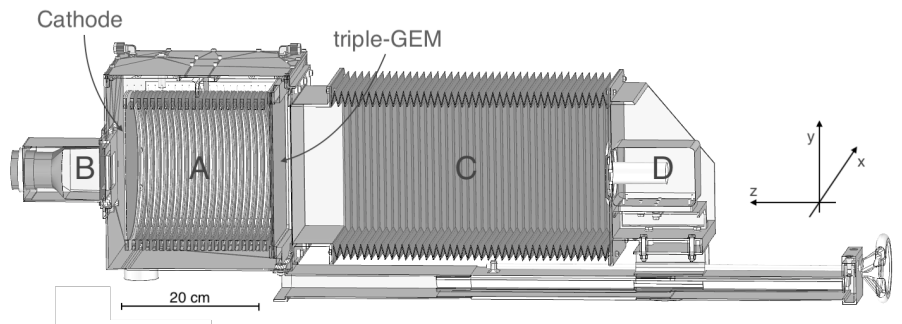


Figure 3. The LEMON prototype [48]. The elliptical sensitive volume (A), the fast photo-multiplier (B), the optical bellow (C) and the sCMOS-based camera (D) are indicated.

195 Measurements with other mixtures are being carried on. In particular, the possible use of small amount of hydrocarbons (e.g. C_4H_{10} or CH_4) to add proton as low mass targets, or low Global Warming Power gases (e.g. HFO) are being tested.

3. Experimental Results with the Prototype

200 The experimental results obtained with the prototype named Long Elliptical MODule: LEMON represents the most comprehensive example currently available of the performance achievable with the CYGNO approach. The LEMON detector, shown in Fig. 3, is schematically composed by:

- a gas sensitive volume of 7 litres contained in a 20 cm long cylindrical field cage (FC) with an elliptical base with 24 cm and 20 cm axes [A];
- a $24 \times 20 \text{ cm}^2$ stack of three GEM as the amplification stage facing the sCMOS camera [D] (optically coupled through a black bellow [C]), being the bottom electrode of the last GEM used as the anode;
- a mesh-based semitransparent cathode closing the volume on the opposite side, behind which a PMT [B] is placed;

210 A more detailed description of this prototype can be found in Ref.[47] and [41]. LEMON standard operating conditions were based on the following sets:

- an He/CF₄ (60/40) gas mixture flux of 200 cc/min;
- an electric drift field within the sensitive volume $E_D = 0.5 \text{ kV/cm}$;
- an electric transfer field in the 2 mm gaps between the GEMs $E_{\text{Transf}} = 2.5 \text{ kV/cm}$;
- a voltage difference across the two sides of each GEM $V_{\text{GEM}} = 460 \text{ V}$;

According to results presented in [43], in this configuration an electron multiplication of about 1.5×10^6 is expected.

As anticipated in Sect. 2.1, high quality cameras are a crucial ingredient for the experiment results. As a result, an ORCA Flash 4.0 camera² was selected to equip LEMON.

²²⁰ This device is based on a $1.33 \times 1.33 \text{ cm}^2$ sCMOS sensor, subdivided in 2048×2048 pixels with an active area of $6.5 \times 6.5 \mu\text{m}^2$ each, with a quantum efficiency of 70% at 600 nm and a readout noise of 1.4 electrons rms. The response and noise level of this sensor were tested with a calibrated light source [33]. A response of 0.9 counts/photon was measured together with a rms fluctuation of the pedestal of 1.3 photons/pixel.

In order to image the large GEMs surface, the camera is equipped with a Schneider lens with 25.6 mm focal length f and 0.95 aperture a . Since at a distance d the lens provides a de-magnification of:

$$\delta = \frac{f}{d-f} \quad (2)$$

²²⁵ the camera optical system is placed at $d=52.6$ cm distance from the GEMs, in order to image a $26 \times 26 \text{ cm}^2$ area. The solid angle covered by the sensor, which in turn determines the geometrical acceptance of photons, is given by

$$\Omega = \frac{1}{(4(1/\delta + 1) \times a)^2}$$

resulting in 1.6×10^{-4} for the LEMON layout.

²³⁰ In order to complement the 2D track projection recorded by the sCMOS with the track trajectory along the drift direction, the arrival time profile of the primary electrons could be extracted from the signal induced on the third GEM bottom electrode. Nonetheless, this is expected (and explicitly shown in [38]) to suffer from a considerably large noise (typically due to jitter on the high voltage supply line), that could prevent signal detection at the low energies at play.

²³⁵ To overcome this limitation, light track time profile was concurrently readout by a Photonics XP3392 Photo Multiplier Tube (PMT) with a 5 ns rise-time, a maximum QE of 12% for 420 nm and a 76 mm square-window, providing sensitivity to single photon and significant reduced noise with respect to the GEM electric signal.

²⁴⁰ The performances of LEMON were tested in recent years at INFN Laboratori Nazionali di Frascati (LNF) overground laboratory by means of radioactive sources (^{55}Fe , AmBe), high energy (450 MeV) electrons from a beam at the Beam Test Facility (BTF, [49,50]) and cosmic rays, and are summarised in the following.

3.1. Operation Stability

²⁴⁵ The performance and long term stability of LEMON was tested for a month long run, during which the detector was exposed to environmental radioactivity, cosmic rays and a ^{55}Fe source [42]. During the whole period, all currents drawn by the high voltage channels supplying the electrodes of the GEM stack were monitored and recorded to identify sudden and large increases that could indicate discharges or other electrostatic issues. During the test, two different kinds of electrostatic instabilities were observed:

- ²⁵⁰ • hot-spots appearing on the GEM surface. While in some cases these would fade out with time, sometimes they started to slowly grow up to tens of nA (on a time scale of minutes). These are very likely due to self-sustaining micro-discharges happening in one or few GEM channels.
- ²⁵⁵ • high charge density due to very high ionizing particles or charge accumulation on electrode imperfections can suddenly discharge across GEM channels. In these events, a sudden increase in the drawn current is recorded with a voltage restoring on the electrodes through protection resistors on a few seconds time basis. Even if these events are less frequent than hot spots, they can be dangerous for the GEM structure and the energy released in the discharge can, in principle, damage it.

² For more details visit www.hamamatsu.com

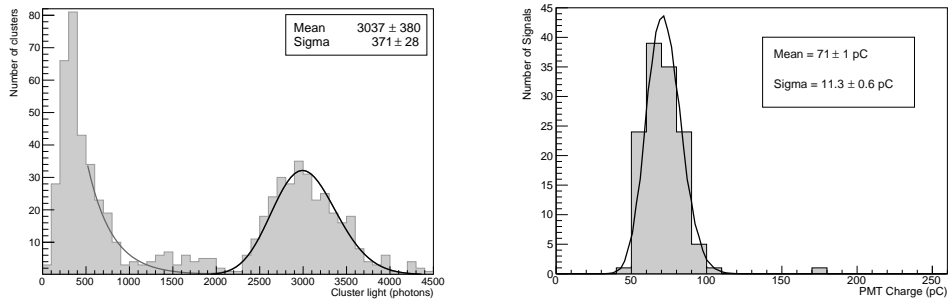


Figure 4. Distribution of the light content of the ^{55}Fe events reconstructed from the sCMOS images (left) and distribution of the charge measured by the PMT signals (right).

260 An automatic recovery procedure was implemented, triggered by the raising of the GEM currents, able to recover both hot-spots and discharges by lowering and gradually restoring the GEM voltages operating conditions in few minutes.

265 An average of 16 of such instabilities per day were observed and the total dead time introduced by the recovering procedures was less than 4%. A detailed analysis of the time interval between two consecutive phenomena did not show any correlation between two subsequent events, nor any increase of their rates. This study demonstrated that the detector operation looked very safe and stable and the obtained performance is considered to be satisfactory. Different gas proportions were tested and a lower amount of CF_4 resulted in a less stable electrostatic configuration.

270 3.2. Light Yield and Energy Resolution

275 The light production was evaluated by analysing sCMOS and PMT response to interactions in gas of 5.9 keV X-rays produced by a ^{55}Fe source. The sCMOS images were acquired in free running mode (i.e. without using any trigger signal) with an exposure of 100 ms. The sCMOS pixels pedestal noise was extracted from the average of 100 images acquired in absence of any light signal and subtracted to each image before the analysis. An elementary clustering algorithm based on nearest neighbor-cluster (NNC) is applied to 4×4 rebinned images to select ^{55}Fe induced energy deposits.

280 Figure 4 shows on the left the light spectrum of the ^{55}Fe events reconstructed from the sCMOS images and on the right the integral of the charge signal measured by the PMT.

The average light yields were evaluated from a Polya fit [51] to the two distributions, resulting in:

- 285 • an average of 514 ± 63 photons per keV were detected by the sCMOS camera (in agreement with results obtained with lower V_{GEM} and E_{Transf} [47]), with an energy resolution of 12%;
- an average of (12.0 ± 0.2) pC per keV with an energy resolution of 16% from the PMT charge signal;

290 The energy resolutions are mainly due to the Poisson's fluctuations of the numbers of primary electrons (8%) and of the gain of the first GEM. The latter term can be simply evaluated to be about 10% by supposing an exponential distribution for it [52], with an average value of 100.

3.3. Detection Efficiency

295 The detection efficiency along the whole 7 litres sensitive volume was studied acquiring sCMOS images varying the position of a collimated ^{55}Fe source in order to vary the x-ray interaction distance to the amplification region and the electric drift field strength within the field cage. Figure 5 shows on the left the number of reconstructed ^{55}Fe spots in the sCMOS images with the algorithm illustrated in Sec.3.2 as a function

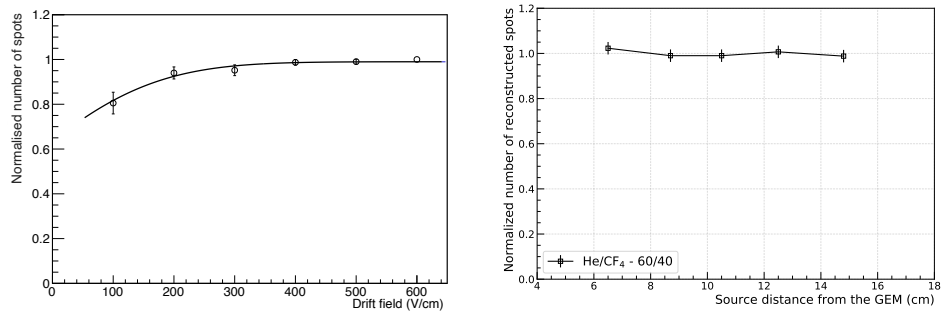


Figure 5. Behavior of the normalized number of ^{55}Fe spots as a function of the drift electric field (left) and event depth in the sensitive volume (right).

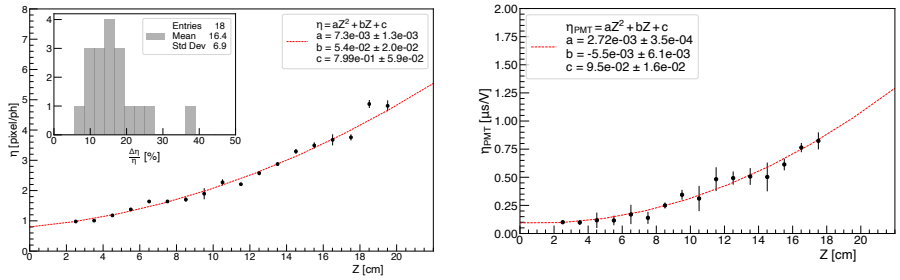


Figure 6. Dependence of η_{light} on left and η_{time} on the right as a function of the track distance from the GEM (see text for details).

of drift field E_D , normalized to the value obtained for $E_D = 600 \text{ V/cm}$. For E_D larger than 300 V/cm a plateau is found, suggesting a full detection efficiency for larger field values. The right panel of Fig. 5 shows the dependence of n on the source distance from the GEM amplification plane, normalised to its average value \bar{n} as measured with a E_D of 600 V/cm . A constant behavior is found in all tested positions, indicating a stable detection efficiency, not dependent on the interaction point distance from the GEM.

3.4. Track absolute distance along the drift direction

The possibility to determine the absolute z position of the energy deposit exploiting the electron drift was studied with 450 MeV electrons from the LNF-BTF facility [41]. The transverse diffusion in the drift gap can in fact be put to use to extract the drift length and thus infer the absolute z distance at which the track occurred.

Seven millimetres long track segments were used to evaluate the detector performance for small energy releases. A position resolution between $100 \mu\text{m}$, near the GEM plane, and $300 \mu\text{m}$, 20 cm far from GEM plane, was found.

As described in [48], the light profile transverse to the track direction possesses a Gaussian shape with the total light L being proportional to $\sigma_{light} \times A_{light}$ (where σ_{light} is the sigma and A_{light} the amplitude of the Gaussian). Because of the attachment effect in gas, the probability for an electron to reach the GEM stack decreases exponentially with a mean free path λ (and thus $L = L_0 e^{-z/\lambda}$). Since σ_{light} is expected to increase as \sqrt{z} because of diffusion in gas, the ratio η_{light} defined as σ_{light}/A_{light} is expected, at a first order approximation, to grow quadratically with the drift distance [41].

Similarly, longitudinal electron diffusion modifies the electron time of arrival on the GEM and thus the time structure of the signal recorded by the PMT. Also in this case, the ratio $\eta_{time} = \sigma_{time}/A_{time}$ between the amplitude and the width of the time waveform is expected to increase with z .

Figure 6 shows the dependence of η_{light} and η_{time} as a function of z with a superimposed quadratic fit.

³²⁵ The inset shows the distribution of ratio between the RMS and the average values of the spectra of η obtained at the various z . These observables can be therefore used to evaluate the absolute z with about 15% uncertainty over 20 cm length [41]. These features result crucial in selecting the fiducial signal volume and therefore rejecting background signals coming from radioactivity of TPC materials, like cathode or GEMs.

³³⁰ *3.5. Detection and Identification of Nuclear and Electron Recoils*

Thanks to the detailed information provided by the high granularity optical sensors, track properties like shape, size, and light density among others can efficiently be exploited to identify and separate Nuclear Recoils (NR), expected from DM signals, from Electron Recoils (ER) coming from background sources.

³³⁵ To quantify these features within CYGNO experimental approach, a track reconstruction and identification algorithm was developed for the analysis of the sCMOS images, called iDBSCAN [53] and based on an adapted version of the well-known Density-Based Spatial Clustering of Applications with Noise (DBSCAN) [54]. The reconstructed clusters were used as seeds for a superclustering algorithm, based on GAC
³⁴⁰ [55,56], which gathers together sub-clusters of the energy deposits belonging to a single track. The GAC, exploiting the number of photons in each pixel as a third dimension to the phase space of the points considered, separately identifies clusters displaying different intensity (i.e. energy deposition patterns), and therefore likely belonging to different classes of particles interactions.

³⁴⁵ The performances of the algorithm were studied on 5.9 keV energy deposits from ⁵⁵Fe and NR produced by an AmBe source [57]. The 5.9 keV_{ee} photons produced by AmBe were nearly completely shielded by a lead shield built around the detector. Data were taken overground at LNF and were therefore highly contaminated by cosmic ray particle interactions.

³⁵⁰ In order to select a pure sample of nuclear recoil candidates produced by the interaction of the neutrons originating from the source and to identify various sources of backgrounds, several cluster shapes observables were exploited. Among these, the *slimness* (ξ) was used to mainly distinguish cosmic rays and the light *density* (δ) to discriminate electron from nuclear recoils. The slimness is defined as the ratio of the
³⁵⁵ Gaussian width of the track in the transverse direction over the projected path length. The density is the ratio of the total number of photons detected by all the pixels gathered in the cluster over the total number of pixels.

³⁶⁰ Exploiting a simple selection on δ , an ER background rejection in the energy region around 5.9 keV_{ee} of 96.5% (99.2%) was found together with 50% (40%) NR efficiency [57].

³⁶⁵ While this cut-based approach is minimalist, and could be improved by more sophisticated analyses combining several topological variables and also the information from PMT waveforms, it shows that a rejection factor larger than 10^2 for electron recoils at $E = 5.9$ keV can be obtained with a gas detector at atmospheric pressure, while retaining a high fraction of NR event signals.

4. The CYGNO experiment roadmap and synergies

The CYGNO project will be developed through a staged approach, to optimise the apparatus and improve its performance while better mitigating any unexpected contingency.

³⁷⁰ This roadmap, comprises:

- PHASE_0: the installation of a large prototype (50 litres of sensitive volume) underground at the INFN-Laboratori Nazionali del Gran Sasso (LNGS) to study its performance in a low background environment and validate MC simulation;
- PHASE_1: testing the scalability of the experimental approach on a O(1) m³ detector while study and minimise the radioactivity background due to apparatus material;

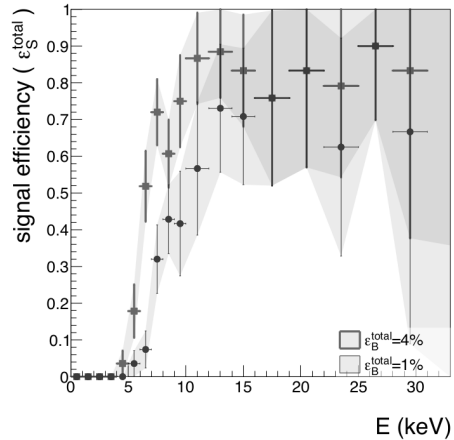


Figure 7. Detection efficiency for nuclear recoils (e_s^{total}) as a function of their detected energy for electron recoils efficiency of 4% (squares) and 1% (circles).

- PHASE_2: according to the results of previous phases, propose a larger scale experiment (30-100 m³) to explore the 1-10 GeV WIMP mass region with high sensitivity for both SI and SD couplings and the possibility of performing the first measurement of low energy solar neutrinos. In both cases the *directionality capabilities* of CYGNO approach will allow not only to detect the interactions, but also to provide useful information for astrophysical studies of incoming particles.

The roadmap details and synergies with other projects will be illustrated in the following.

4.1. CYGNO PHASE_0: the LIME prototype

The PHASE_1 demonstrator will be based on readout modules having the LIME dimensions and layout. For this reason, its successful assembly and operation will be paramount to substantiate the efforts and confirm the scientific and technological choices towards the 1 m³ detector.

The Long Imaging ModulE (LIME, in Fig. 8) is the larger prototype foreseen to conclude the R&D phase of the project. It was conceived to have the same drift length (50 cm) of the final demonstrator (Sect. 4.2) and the same the readout scheme based on a triple 33 × 33 cm² thin GEMs (stretched on plexiglass frame to reduce radioactivity) imaged by a single sCMOS sensor and 4 small PMT symmetrically placed around the sensor, at a distance of about 15 cm from it and 25 cm apart from the GEM surface. The new Hamamatsu ORCA-Fusion Camera was employed³ with improved performance with respect to the Orca Flash in terms of reduced noise (0.7 versus 1.4 electrons per pixel), larger number of pixels (2304 × 2304 versus 2048 × 2048) and larger quantum efficiency (80% versus 70% at 600 nm). The choice of 4 PMT resides in the possibility of better reconstructing the track position and inclination through the center of gravity of the light signal from the 4 sides, strongly mitigating any possible pile up effect.

The gas volume is enclosed in a 10 mm thick plexiglass box, that provides gas tightness. The field cage is composed by copper rings, conveniently roundly shaped to avoid discharges, at a 16 mm pitch.

In its underground installation LIME will be equipped with the same DAQ system and gas system envisaged to be employed for the realisation of PHASE_1, currently under test.

³ <https://www.hamamatsu.com/eu/en/product/type/C14440-20UP/index.html>

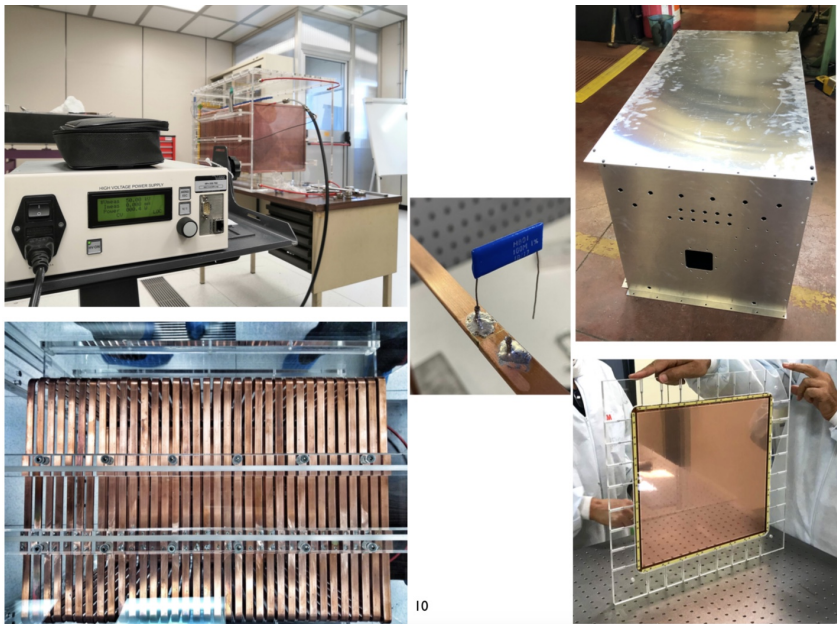


Figure 8. Pictures of the LIME detector assembly at LNF: top left with drift field and GEM operating at nominal voltages, bottom left detail of the field cage copper rings, center detail of the resistor soldered to the field cage ring, top right LIME inside the Faraday cage, bottom right detail of the triple GEM stretched with pullouts on a plexiglass frame.

A response of about 650 ph/keV was measured that has to be compared with 514 ph/keV obtained with LEMON (see Sec.3.2) thanks to the larger sensitivity of the Orca Fusion camera. The low sensor noise (about 1 photon/pixel), will allow to operate with an effective energy threshold of hundreds of eV. The energy resolution on the ^{55}Fe peak is measured to be 14% across the whole 50 cm drift length, with full efficiency in the full 50 litres volume. LIME has been furthermore already operated for one entire month in He/CF₄ 60/40 at 1 atm, with its currents continuously monitored and logged, showing comparable stability to LEMON (see Sec.3.1).

The installation at LNGS, completed with the PHASE_1 auxiliary systems, will allow:

- to test the detector performance in low radioactivity and low pile-up configuration;
- to characterise the real radioactive background present in the site and then to validate the GEANT4 simulation;

420 4.2. CYGNO PHASE_1: the $O(1)$ m³ demonstrator

After having optimised and assessed all technological aspects with LIME underground tests, project will move to PHASE_1, with the aim of studying and minimising material radioactivity effects on a real experiment scale and therefore evaluate its sensitivities.

425 The exact PHASE_1 detector size will depend on the available underground site, that is still under discussion; anyway a 1 m³ active volume will be discussed in this paper, schematically shown in Fig. 9, with the consideration that the foreseen layout and auxiliary system can be directly and easily adapted to the definitive detector dimensions.

The active volume of the detector will be contained in a gas volume vessel (GVES), 430 realized with PMMA to lower the material intrinsic radioactivity, reduce the gas contamination, and ensure the electrical isolation from cathode and field cage. The GVES will contain two field cages 500 mm long, with two back-to-back TPCs separated by a central aluminised mylar cathode following the DRIFT example [58–60]. This foil is expected to minimise backgrounds induced from recoils by the decay chain of radon.

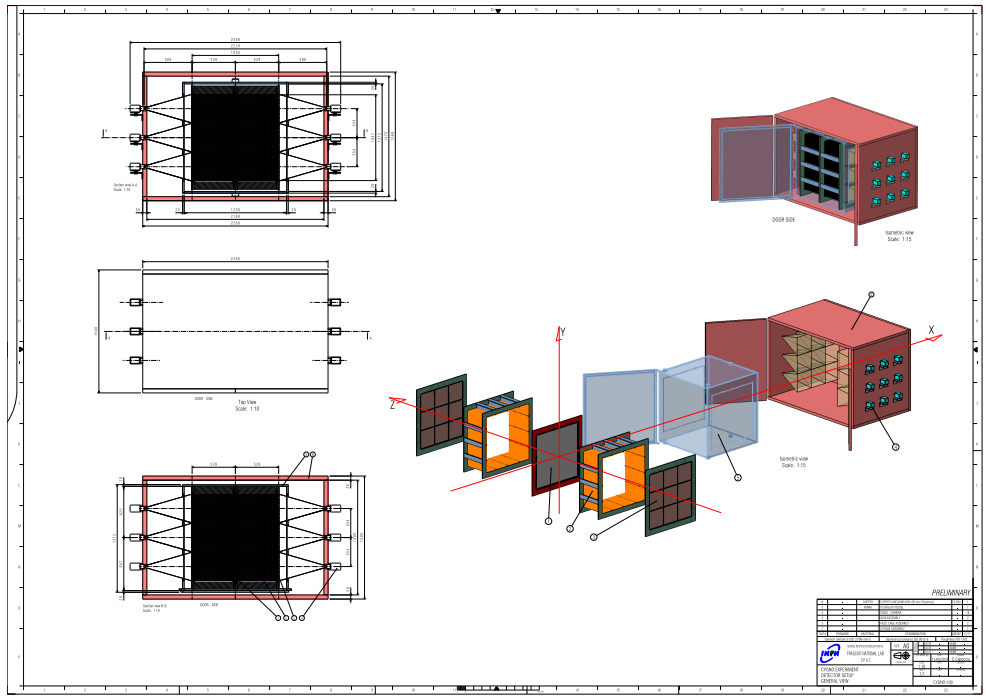


Figure 9. CYGNO PHASE_1 Sensitive Detector Layout.

435 Each of the 2 end-caps will have an active area of 1 m^2 surface, readout by a matrix of 3×3 modules of $33 \times 33 \text{ cm}^2$ area, each one equipped with a stack of three GEMs, 1 sCMOS and 4 PMT, identical to the LIME prototype (see 4.1).

440 The GEMs will be assembled adapting the technique discussed in [61]. The mechanical rigidity will be provided by the outer frame that will be anchored to the GVES. The assembled GEM stack will be inserted into the GVES through vertical slits, which will allow an easy substitution of a single GEM foil in case of damage.

The high voltage system has been conceived with the assumption of independent lines for each electrode of the GEM foils, in order to ensure safe and reliable operation of the detector modules.

445 The DAQ system will be able to collect synchronized data from cameras and photodetectors and to handle the following specifications:

- camera exposure from 0.2 to 1 second (1 to 5 Hz frame rate);
- 10 MB of data per picture (5 MP, 16 bits/pixel);
- 12-bit digitization of photodetector waveforms at $\sim 250 \text{ MS/s}$ in $\lesssim 1 \mu\text{s}$ windows.

450 Fast responses provided by the PMT will be exploited to trigger the acquisition of sCMOS sensors. Different possible trigger scheme are under evaluation along with the possibility of running either in trigger or trigger-less mode.

The acquisition will be distributed through a redundant system of machines to ensure the system stability. To acquire fast photodetectors, digitization boards are 455 considered. In this scenario, the bottleneck for the acquisition would be the throughput to the disk, typically limited to $O(200 \text{ MB/s})$, and some preselection of the images by a farm of CPUs would be needed.

4.2.1. PHASE_1 Shielding Scheme and Material Budget

A GEANT4 based Monte Carlo simulation of the whole apparatus in Fig. 9 has been 460 developed to study detector backgrounds and to optimise the choice of shielding and materials.

The effect of the diffused environmental gamma rays and neutron flux was studied. Different configurations of external passive shielding with layers of copper, lead and water were studied with the goal of having less than 10^4 photons/year interacting

Component	^{238}U (^{234m}Pa)	^{238}U (^{226}Ra)	^{235}U	^{232}Th (^{228}Ra)	^{232}Th (^{228}Th)	^{40}K
Camera body [Bq/pc]	7	1.8	0.4	2.1	2.1	1.9
Camera lens [Bq/pc]	0.9	0.41	0.031	0.08	0.08	11
GEM foil [Bq/m^2]	< 0.104	0.004	< 0.002	< 0.004	< 0.002	< 0.045
Acrylic [Bq/kg]		0.003		0.005	0.004	0.035

Table 1: Measured activity of the internal detector components expected to produce the largest backgrounds in the active volume. The isotopes in parentheses indicate the activity from that particular part of the decay chain. Upper limits are given at 90% confidence level.

465 in the target gas between 1 keV and 20 keV. The choice of this benchmark is backed up by indication from measurements [62,63] and simulations within the CYGNUS collaboration[19] that a TPC with 3D readout can reach a 10^5 gamma/year rejection factor at O(keV).

470 While the use of lead can significantly reduce the overall setup dimensions, the simulation showed that this configuration would require archaeological lead in order not to induce additional background from the shielding, therefore largely raising the cost of this layer. A cost-benefit optimisation of the shielding materials and thicknesses was hence developed, identifying 2 m of water + 5 cm of copper as the optimal configuration. This shielding provides an attenuation of about a factor of 10^{-7} for external photons and 475 5×10^{-5} for external neutrons, reducing the number of expected electron recoils in the active volume below 10^3 cpy (with O(1) cpy nuclear recoils) in the range 1-20 keV.

480 For the evaluation of the backgrounds generated by detector materials, the natural photon radioactivity of the components expected to give the largest contributions was experimentally measured with high purity Germanium detectors thanks to the support of LNGS Special Techniques Service and are reported in Table 1.

485 Regarding the GEMs, the major source of background is found to come from the frames rather than the foils themselves. For this reason, in the LIME prototype of PHASE_0 the triple $33 \times 33 \text{ cm}^2$ GEMs were mounted and stretched on low radioactivity acrylic frames, with the same technique foreseen to be applied to the PHASE_1 detector.

490 For what concerns the sCMOS optical system, a large ^{40}K contamination was observed in the lens glass. Suprasil was selected as an alternative material for the fabrication of the lens, for an expected $\sim 10^4$ reduction of the contribution from this item. An overall activity of less than 50 mBq/kg was found in recent measurements performed on a sample at LNGS, confirming the very good properties of this material.

495 sCMOS cameras have never been employed yet in DM searches, and therefore their intrinsic radioactivity has never been studied or optimised in this context. For this reason, an extensive program working in close contact with sCMOS camera producer companies and with LNGS Services to assess this aspect within our experimental approach has started. Gamma spectroscopy of several sCMOS cameras as a whole was performed, including models from companies different from Hamamatsu, and verified that all display similar activities in the O(10) Bq/piece. The measured activities of the Hamamatsu Orca Fusion are shown in Table 1. A camera was disassembled in 20 different pieces, which are currently under measurement in order to pin point the components introducing the largest radioactivity contamination and possibly replace them by cleaner options. Given 500 the very large sCMOS activity, in the PHASE_1 design they are foreseen to be shielded by the 5 cm copper layer on all sides, except for the one facing the GEM.

505 Starting from these considerations, a background evaluation for a 1 m^3 PHASE_1 detector was developed, that includes the external gamma and neutron flux contribution with the copper and water shielding discussed above, and the radioactivity contribution of the main internal components. For the latter, the values measured at LNGS for GEMs, camera lens, camera body and acrylic for the gas vessel, and data from literature for the Cu of the cathode and the field cage rings [64] were employed. This study showed that O(10^3) nuclear recoils and O(10^6) electron recoils per year are expected in the sensitive

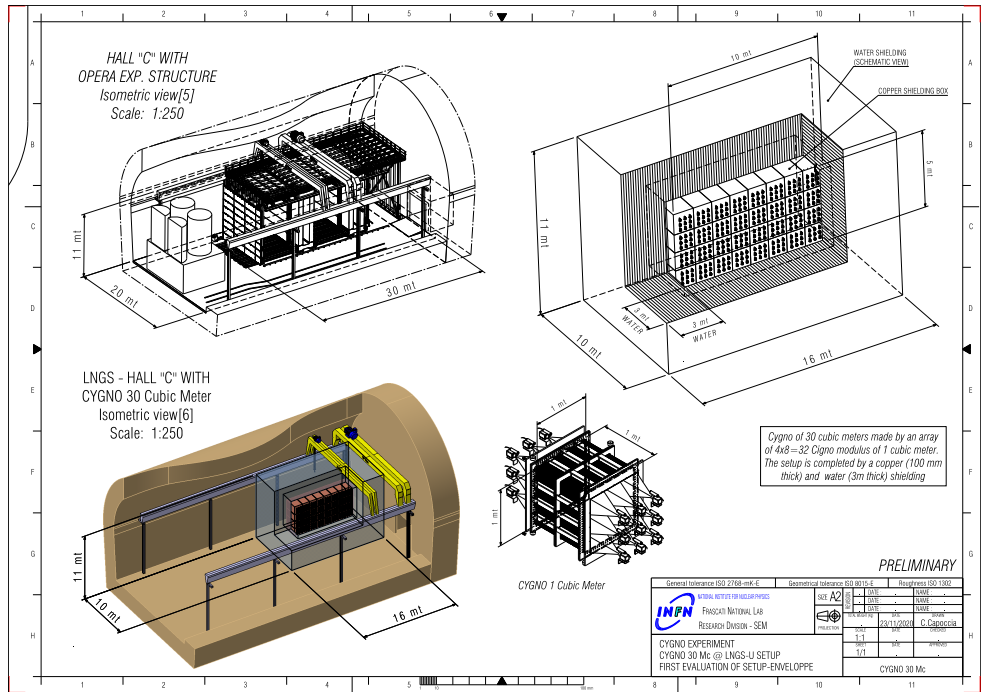


Figure 10. CYGNO PHASE_2 possible setup.

volume, with energy in the 0–20 keV range. It must be noticed that all the nuclear recoils are produced by the GEMs and are absorbed in the gas within 5 cm from them. As it is described in Sect. 3.4, by exploiting the effect of diffusion in gas, the track absolute distance from the GEM can be evaluated with a resolution better than 20%. Therefore, this NR background is expected to be reduced to zero with a suitable selection on the drift distance, without a significant reduction of the detector fiducial volume. Apart from the current lens, the largest amount of electron recoils is produced by the sCMOS cameras, and, at a second order, by the GEMs.

This study represents the current evaluation of the expected backgrounds for a 1 m³ detector. Therefore it is the starting point for the optimisation and assessment of the background level which will be further minimised by the detailed study of the GEM, sCMOS and optics materials.

4.3. CYGNO PHASE_2

A CYGNO detector with a volume of the order of several tens of cubic meters would be able to give a significant contribution to the search and study of DM in the mass region below 10 GeV, both for SI and SD coupling. In case of appearance of signals or evidence of interactions not due to ordinary matter, the information provided by a directional detector (interaction position, incoming particle direction and energy) will be fundamental to positively confirm the Galactic origin of the detected signal as DM and determine its origin and properties.

Such a detector could furthermore provide the first directional measurement of Solar neutrinos from the pp chain, possibly extending to lower energies the Borexino measurement, as it will be illustrated in Sec. 5.3.

As an example, Fig. 10, shows how a 30 m³ sensitive volume apparatus with all its shields (for a total volume of 2×10^3 m³) would fit into LNGS experimental Hall C.

The development of such a detector in terms of intrinsic background minimisation, performance and costs would of course require an improved scalable design, materials and readout. The possible improvements include, but are not limited to, the following:

- development of custom sCMOS sensors, with features focused on CYGNO requirements: low noise, high sensitivity and reduced intrinsic radioactivity together with a lower production cost;
- 540 ● design and realisation of low radioactivity lenses with fixed focus and large aperture;
- reduction of the intrinsic detector material radioactivity, with the lesson learned after the results obtained with PHASE_1;
- development of innovative gas mixtures for optical readout (illustrated in the
- 545 following sub-sections) to boost the tracking performances and improve sensitivity for low energy releases.

4.4. Hydrogen rich gas mixtures

The presence of low mass nuclei as targets in the gas mixture improves detector performance mostly in the low DM mass region:

- 550 ● momentum transfer is more efficient as shown in eq. 1;
- longer length of light nuclear recoils in gas producing tracks more easy to detect and with a clearer direction.

The collaboration is studying the effect of the addition of a small percentage of iC₄H₁₀ (1%-5%) to the He/CF₄ gas mixture. First results demonstrate that, even if the 555 number of photons collected per keV released decreases up to a factor 3 (with a 5% addiction) light signals are still clear and well visible. Studies on this and other hydrogen rich mixtures are still going-on and represent a very promising opportunity to lower the effective DM mass threshold.

4.5. INITIUM: an Innovative Negative Ion Time projection chamber for Underground dark Matter searches

The challenging goal of INITIUM is to develop Negative Ion Drift (NID) operation within the CYGNO optical approach.

Negative Ion Drift is a peculiar modification of conventional TPCs (NI-TPC) that involves the addition to the gas of a highly electronegative dopant [65,66]. In this 565 configuration, primary electrons liberated by the track while ionising the gas are captured at very short distances <10-100 μm by the electronegative molecules, creating negative ions. These anions drift to the anode, where their additional electron is stripped and gives rise to a standard electron avalanche. Since anions mobility depends on the mass, the difference in the time of arrival of different anions effectively provides a measurement 570 of the position of the event along the drift direction. Full 3D detector fiducialization can be obtained exploiting this information (i.e. DRIFT), and background-free operation over 1 m³ [67]. Thanks to these two features, NI-TPC readout planes can image a larger volume than conventional TPC approaches, resulting in lower backgrounds and costs per unit mass.

The SF₆ compound has been recently demonstrated to work very well as negative ion gas between 20 and 100 Torr, including the possibility of high gains and fiducialization via minority charge carriers [68–70]. Compared to the high vapour pressure, low flash point and low explosive mixture in air of the CS₂ employed by DRIFT, SF₆ has the substantial advantages of much more safer handling, combined with easier Radon 580 purification and re-circulation, while at the same time increasing the target fluorine mass. The studies proved for the first time the feasibility of NID at nearly atmospheric pressure (0.8 atm) with He/CF₄/SF₆ at 360/240/10 Torr with triple thin GEMs and charge pixel readout (Timepix) [71].

INITIUM goal is to develop a scintillating He/CF₄/SF₆ based gas mixture at atmospheric pressure with low content of SF₆ for NID within optical readout. If NID can be achieved within the optical approach, tracking could be improved by the possibility of reconstructing the track shape along the drift direction by sampling the recorded light at a kHz frame rate. At the moment such high rate can be met only by cameras

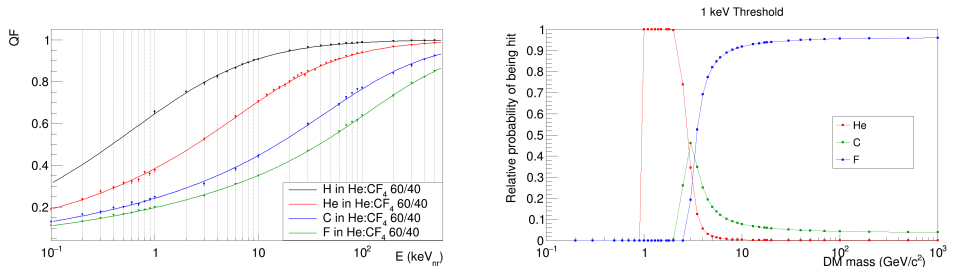


Figure 11. Left: quenching factor values for different elements in a 60/40 He/CF₄ as a function of the nuclear recoil energy E[keV_{nr}]. Right: relative probability of nuclear recoils being detected as a function of the DM mass. The energy threshold is 1 keV_{ee} and the quenching factor corrections are included.

with low resolution and high noise, not yet suited for low energy rare events searches.
590 Nonetheless, given the fast development of the sCMOS technology, progresses in short time are possible which could open the door to this possibility.

5. CYGNO Scientific Goals and Expected Physics Performances

5.1. WIMP-like DM searches at low masses through nuclear recoil signature

A statistical analysis based on the Bayesian approach to evaluate a CYGNO PHASE_2
595 30 m³ experiment sensitivity to WIMP searches in presence of background was performed.

The CYGNO approach allows to measure both the energy and the direction of the track simultaneously, and both the information will be combined to evaluate the number of detected events for the final analysis. Nonetheless, since the angular distribution
600 discriminating power is significantly stronger than the energy spectrum shape, this sensitivity study focuses only on the first one for the sake of simplicity. In addition, the background angular distribution can be reasonably assumed to be isotropic in Galactic coordinates, while its energy spectrum will highly depend on the exact materials and shielding employed in the experiment and therefore difficult to predict with precision at
605 this stage of the project development.

The energy threshold plays however an important role in the determination of the signal angular distribution, together with the target nuclei. In this sensitivity study, two energy thresholds were assumed: a realistic 1 keV_{ee}, backed up by the published results
610 [47], and an optimistic one of 0.5 keV_{ee}, extrapolated from the improved performances obtained with PHASE_0 LIME prototype (see Sec.4.1). In order to translate this into nuclear recoil energy, a SRIM simulation was developed to evaluate the quenching factor (QF) for the elements in our gas mixture, including Hydrogen given the discussion in Sec.4.4. The QFs for H, He, C and F in He/CF₄ 60/40 at 1 atm as a function of the nuclear recoil energy E[keV_{nr}] are shown on the left of Fig. 11. This results in an effective energy threshold of 2.13 (1.23) keV_{nr} for He, 3.13 (1.80) keV_{nr} for C and 3.80 (2.17) keV_{nr} for F for 1 (0.5) keV_{ee} energy deposit.

The signal angular distributions were hence calculated with these effective thresholds in Galactic coordinates, starting from [72–74] and neglecting the motion of the Earth as it was shown to have secondary relevance on the angular distribution. Possible shapes of a DM signal nuclear recoil distribution are shown in 2D Galactic Coordinates in Fig. 12, where it is clearly visible its an-isotropic nature. The final shape of the distribution strongly depends on three elements: the DM mass, the element hit and the energy threshold. With the chosen settings for the analysis, the angular distributions tend to be strongly peaked at low masses and more spread at heavier masses, where there is no angular region forbidden by kinematics.
625

In order to establish the Credible Interval (CI) of the sensitivity limits, fake experiments are simulated by extracting events according to the expected measured angular distributions discussed so far, adding detector effects. Since CYGNO's approach direc-

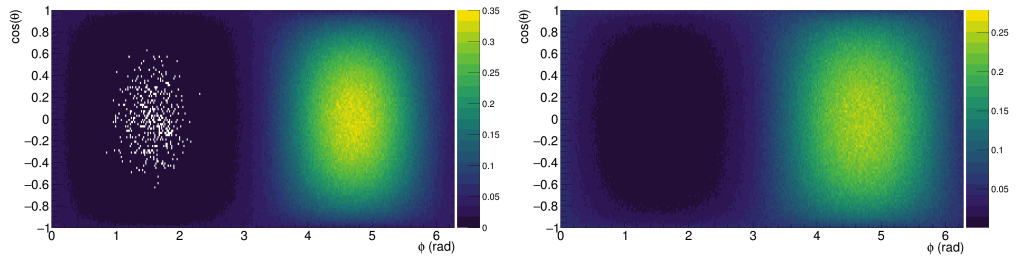


Figure 12. Two examples of the angular distribution of recoils due to DM in Galactic coordinates, obtained by Monte Carlo simulations. On the left helium recoils induced by $10 \text{ GeV}/c^2$ DM. On the right fluorine recoils induced by $100 \text{ GeV}/c^2$ DM.

tional capabilities are still under evaluation, for this study an angular resolution of 30° in the whole detectable range is assumed, as from literature [75] and from the CYGNUS simulation [19], with full head-tail recognition down to the 1 keV_{ee} energy threshold.

A simple flat distribution of the number of expected signal events between 0 and 1000 is used, given that articulated signal prior probabilities can not be assumed without risking biases, being the actual cross section of DM with protons unknown. Indeed, events per year is a non negative defined variable and due to current limits in the DM community, it is hardly believable that more than 1000 events per year would be produced in the CYGNO detector.

The number of expected background events for CYGNO PHASE_2 can not easily be predicted at this stage of the project, since it will depend on the outcome of PHASE_0 and PHASE_1 and the possible improvements discussed in Sec. 4.3, 4.5 and 4.4. For this reason, different possible background scenarios are simulated, with 100, 1000 and 10000 events per year. For these, a Poissonian prior is used, since the measurements with PHASE_1 and simulations informed from these results will allow in the future to obtain a guesstimate of the background yield.

For each scenario, the actual number of events is randomly extracted from this Poissonian distribution and a direction is assigned to each, randomly sampling the background angular distribution. After applying a Gaussian smearing to account for the resolution, an histogram representing the measured event direction in Galactic coordinates is filled, with its binning reflecting the angular resolution. In the hypothesis of only background, no events for the WIMP-induced signal recoils are added. In order to avoid suffering from any underfluctuation of the background (as undersampling), 500 data samples are simulated and the average result is taken as final value.

The likelihood of the detected events to be the sum of background plus signal (see Sec. A for details) is evaluated on each data sample. From these, the posterior probability at 90%CI of the number of WIMP-induced recoil is computed, and averaged to obtain the final result.

In order to translate this into a limit in the cross section versus mass parameters space, it is important to take into account that, being the target a mixture of different elements, both the kinematic of the expected DM-nucleus interactions and the expected rate calculation influence the probability of each element to be detected differently as a function of the DM mass. This is shown on the right of Fig. 11 for a 1 keV_{ee} energy threshold. The region of the DM velocity distribution accessible to detection is limited at lower values by the energy threshold and at higher by the local escape velocity (here taken as 544 km/s [76]). Thus, at lower DM masses, being the window of DM velocity distribution accessible very small, the detection of an element is strongly susceptible to its energy threshold. Therefore, Helium detection dominates the early part of the figure and the rising probabilities of Carbon and Fluorine reflect their different thresholds. At higher DM masses, when the window is quite large, the A^2 cross section enhancement (where A is the atomic number) dominates, making fluorine the most probably detectable element. Figure 11 displays also the minimum DM mass detectable by each element with

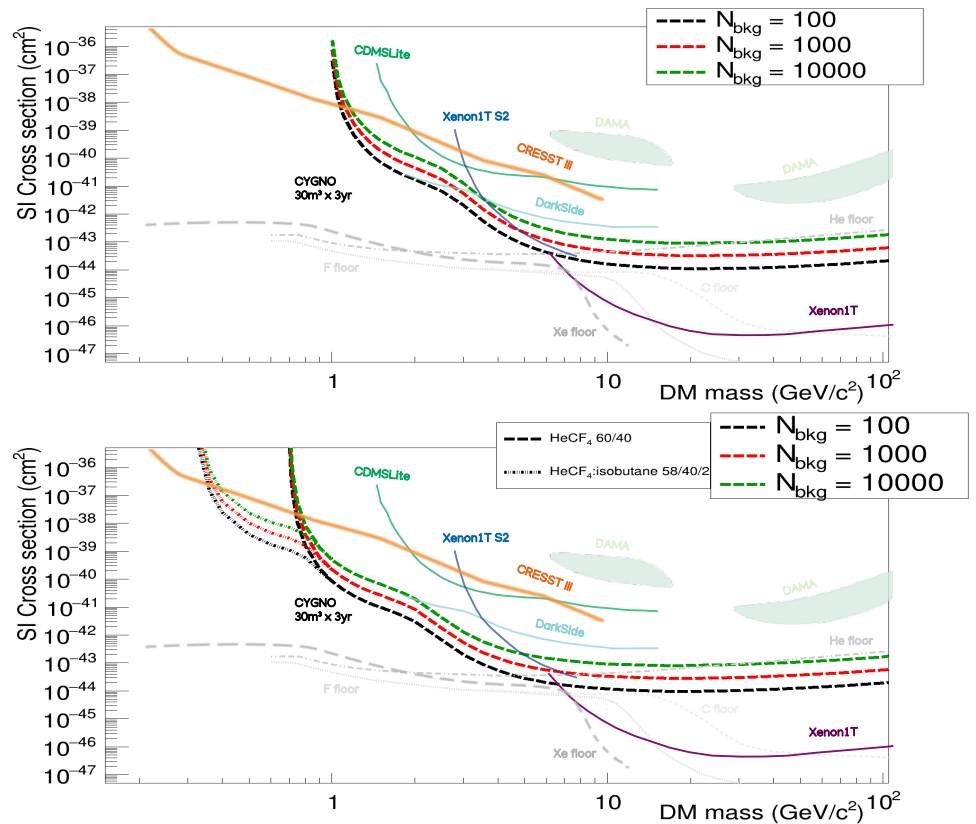


Figure 13. Spin Independent limits for WIMP-nucleon cross section for 30 m^3 CYGNO detector for 3 year exposure with different background level assumptions. The line representing other experiment and neutrino floor levels are taken from [77–83].

a 1 (0.5) keV_{ee} energy threshold, that is 0.97 (0.69) GeV/c² for He, 1.89 (1.38) GeV/c² for C and 2.55 (1.87) GeV/c² for F recoils.

Figure 13 shows in the top part the expected SI limits for a 30 m^3 CYGNO PHASE_2 experiment for 3 year exposure with different background scenario and 1 keV energy threshold, while the possible regions explored with a operative threshold of 0.5 keV are shown in Fig. ?? bottom together with the results that can be reached with a gas mixture hydrogen-rich with 2% Isobutane content, as discussed in Sec.4.4.

The shape of the limit reflects the different nuclear composition of the gas mixture. The lower DM mass detectable obviously corresponds to the one obtainable with 0.5 keV_{ee} energy threshold and Helium quenching factor (Hydrogen in the hypothesis of the addition of a small fraction of Isobutane). There is a kink on the curve at around 0.9 GeV/c², corresponding to the transition from Hydrogen dominated to Helium dominated recoils, and at 3 GeV/c² from Helium to Fluorine dominated recoils. The Carbon percentage on the total gas mixture (8%) is too low to produce a visible effect on the curve.

Figure 13 shows how all the scenarios considered in this sensitivity evaluation will be able to probe regions in WIMP masses versus cross sections plane not yet explored to these days, therefore significantly contributing to future DM searches for low WIMP masses. While it is true that the expected reach of future realisation of SuperCDMS [84], CRESST [85], Darkside 50 LowMass [86] and NEWS-G experiments will be able to cover these regions, all of these will be realised through modes of operation that strongly reduce (if not even completely give up) means for background discrimination. Each of these approaches implies therefore very strict (and not yet demonstrated) requirements on the detector materials radio-purity and the capability to strongly rely on a precise estimate of the expected backgrounds. As a consequence, any observed signal in this region by

these experiments will be difficult to interpret unambiguously as DM signal. CYGNO potential of establishing the galactic origin of the detected signal through directional correlation with the Cygnus constellation would therefore constitute a compelling and decisive test to any experiment claim in this region, being the only existing approach
⁷⁰⁰ able to provide a positive identification of a DM signal. CYGNO PHASE_2 realisation would moreover establish the grounds for the development of the multi-site network of modules for a ton-scale CYGNUS project, that through directionality could perform a precise study of WIMP properties and DM astronomy.

In addition, thanks to the high Flourine content, CYGNO PHASE_2 results to be
⁷⁰⁵ significantly sensitive also to SD couplings, able to explore regions not yet excluded by the Pico experiment in the low background scenario, as shown in Fig. 14. The PICO experiment, that possesses the strongest sensitivity among all the existing and planned experiments exploring the SD coupling, is based however on an energy threshold approach. This implies that signal observation does not allow to measure the energy
⁷¹⁰ of the detected nuclear recoil and could not therefore be translated into a constraint in the masses versus coupling parameter space. Hence, also in this context, not only a confirmation of the galactic origin of the detected signal would be necessary, but it would result imperative in order to establish the detected WIMP properties, that are not attainable through PICO experimental approach alone. Moreover the possibility, now
⁷¹⁵ under study, of running with a threshold of 0.5 keV, would allow to reach DM masses even lower than what is expected for the upgrade of PICO.

The estimated sensitivities presented in Fig. 13 and Fig. 14 demonstrate how CYGNO PHASE_2 realisation would therefore constitute a very important and compelling step towards the observation and study of a DM signal in the low WIMP mass
⁷²⁰ region for both SI and SD couplings.

5.2. Directional searches for MeV Dark Matter produced by Supernovae through nuclear recoil

While WIMPs still remains highly motivated DM candidates, they are not the only paradigm that can explain the observed DM presence. Core-collapse supernovae (SN) can reach core temperatures in excess of 30 MeV for O(10) seconds, allowing
⁷²⁵ them to produce vast thermal fluxes of particles with masses O(100) MeV at relativistic speeds [91]. This makes them an ideal astrophysical source for sub-GeV dark matter. The DM candidate emerging from this scenario considered in [91] are dark fermions, but this is not the only possible realisation of such mechanism. Such particles end up diffusively trapped near the proto-neutron star that forms from the SN core. The dark fermions that
⁷³⁰ do eventually escape are produced with a velocity distribution approximately Maxwell-Boltzmann with semirelativistic velocities ($v \sim 1$, to be compared to classical WIMPs with $v \sim 10^{-3}$), exhibiting a roughly order-one spread in velocities. This will results in a time-spreading effect during their propagation to Earth up to 10^5 years for an average galactic SN, creating an overlap in time of various SN. Given the high SN concentration in the galactic center, the emission of > 100 SN is expected to be overlapping in a diffuse flux at
⁷³⁵ Earth at any given time. This resembles the diffuse flux of SN neutrinos comprising to the Neutrino Floor at energies larger than 10 GeV WIMP masses.

Thanks to the large dark fermion momentum, such particles, even being of mass of O(10 MeV), would cause in a detector on Earth a measurable nuclear recoil of O(keV)
⁷⁴⁰ very hard to distinguish from the one induced by a classic WIMP of the Galactic halo by an experiment measuring only the energy deposited in the active volume. Nonetheless, the expected diffuse flux will be strongly peaked towards the Galactic center, due to the large presence of SN in this region compared to extragalactic sources. Thanks to this high degree of anisotropy, directional detector results in a crucial tool to discriminate MeV SN-
⁷⁴⁵ produced DM with respect to classical WIMP scenarios. It has in fact recently been shown that a directional approach with realistic experimental performances could distinguish the two scenarios with few detected signal events, typically between 1 to 2 order of magnitude with respect to the yield needed by a non-directional detector [16]. While

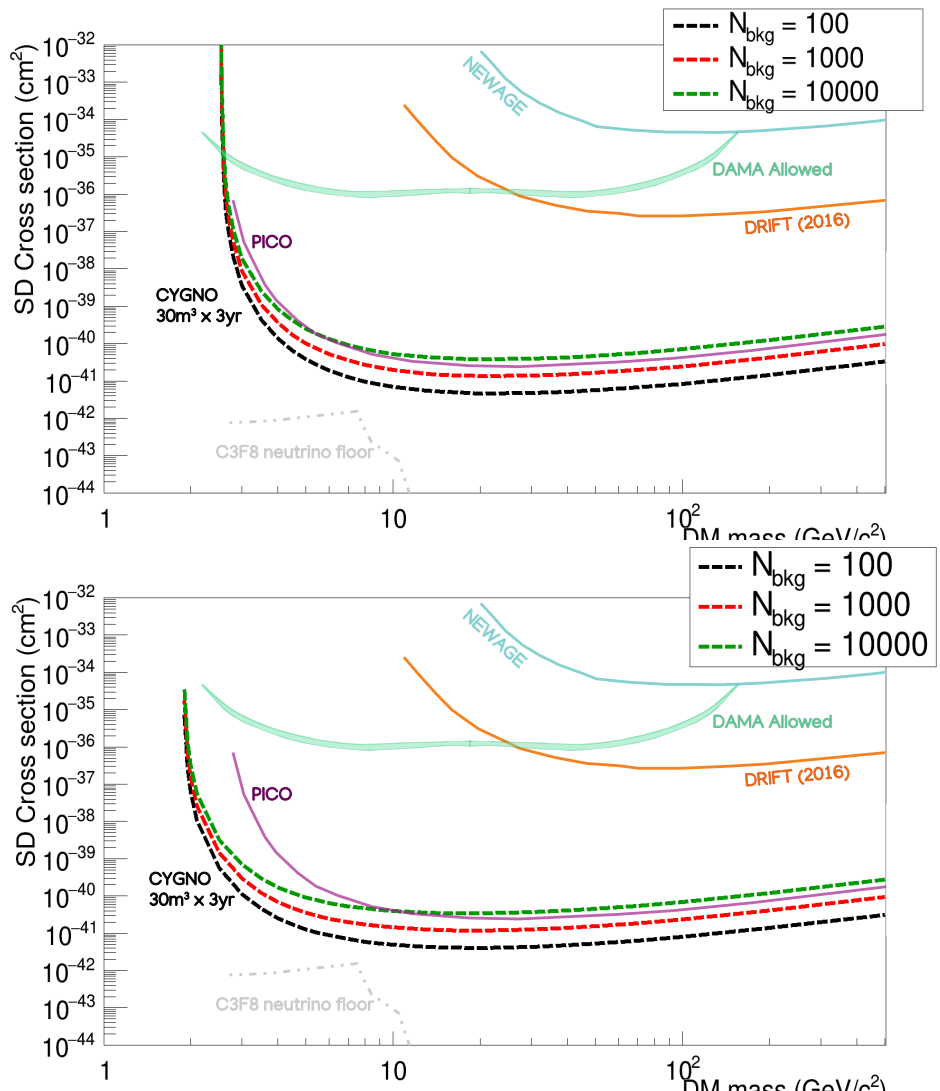


Figure 14. Spin Dependent limits for WIMP-proton cross section for 30 m³ CYGNO detector for 3 year exposure with different background level assumptions for an operative threshold of 1 keV (top) and 0.5 keV (bottom). The line representing other experiment are taken from [87–90].

this study was performed under the assumption of absence of background in the detect
750 events, a full estimation of CYGNO sensitivity to this DM candidate scenario with the tools discussed developed for the WIMP physics case in Sec.5.1 is under development.

5.3. Solar neutrinos detection through both nuclear and electron recoil signature

Solar neutrinos are well known background to DM searches. They can interact in the active volume of the detector either via elastic scattering on the electrons (producing an electron recoil) or coherent scattering on the nuclei (producing a nuclear recoil).
755

Since most of current DM experiments possess ER/NR discrimination, typically only the coherent scattering on nuclei is viewed as an irreducible source background, as is in fact denominated "Neutrino Floor". Directionality has been extensively recognised as the preeminent tool to identify and discriminate NR induced by Solar neutrino from
760 WIMP signal event [2,19,92]. While a ton-scale experiment is needed to start detecting these events [19], due to the low cross section, new physics in the neutrino sector (described in terms of new mediators between neutrinos and electrons and/or quarks or in terms of non standard effective interactions) can increase the rate at low energies [93,94]. This is particularly true for DM mass below 10 GeV, if a new scalar mediator is

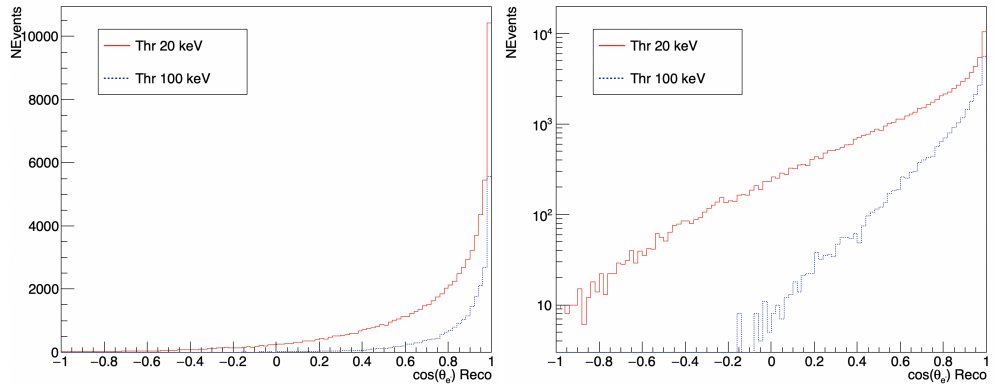


Figure 15. Angular distribution for electron recoils induced by Solar neutrinos for 20 keV and 100 keV energy threshold with a $30^\circ \times 30^\circ$ angular resolution, on the right in log scale.

assumed, where the neutrino floor can be raised by several orders of magnitude, making this accessible to CYGNO PHASE_2.

For what concerns ER induced by neutrino-electron elastic scattering, classical DM experiments measuring only the deposited energy in the detector have no means to discriminate them from ER caused by other sources, and hence treat them as background. Detector exhibiting directional capabilities like CYGNO can actually transform these events into a signal. From the ER direction and the Sun position, the angle between the incoming neutrino and the scattered electron can in fact be inferred, providing an unambiguous signal identification just like with the one in directional WIMP searches. Ton-scale gaseous TPC have already been proposed in the past [17,18] to perform Solar neutrino spectroscopy. The CYGNO CF₄ based gas mixture appears very attractive in this sense [18], because it possesses a significative electron density ($1.05 \times 10^{21} \text{ cm}^{-3}$) with a low Z nuclei, a feature that maximises the number of targets while minimising the multiple scattering.

About 1 event/m³ per year is expected at atmospheric pressure for an ER energy threshold of 20 keV coming from the pp chain, making this an extremely interesting physics case for CYGNO PHASE_2 experiment. Due to the larger multiple scattering suffered by low energy electron with respect to nuclei, ER direction determination results more complex than with NR tracks. First results from a dedicated algorithm developed within the collaboration, inspired from X-ray polarimetry [95], shows that 30° 2D angular resolution with sense recognition larger than 80% from the sCMOS images analysis can be achieved at 20 keV in a 1 m³ detector, improving at higher energies. Figure 15 displays the angular distribution for ER induced by Solar neutrinos for 20 keV and 100 keV energy threshold with a $30^\circ \times 30^\circ$ angular resolution. Since background events will be isotropically distributed, this shows how even with the limited angular resolution assumed, directionality provides an extremely effective means for high precision solar neutrino measurement. Moreover, the 20 keV energy threshold assumed for the ER translates in about 80 keV threshold on the incoming neutrino, opening a new window of opportunity on the pp Sun process down to low energy, unreachable to conventional neutrino detectors[17].

6. Conclusions

In this paper, the case for directional DM searches with gaseous TPC with optical readout through the combination of sCMOS images and PMT signals is presented. The performances achieved with a 7 litre prototype based on this approach show the possibility of $O(\text{keV}_{nr})$ detection threshold with 10^2 ER/NR discrimination at 5.9 keV_{ee}. The CYGNO experiment will develop through a staged approach, where the underground installation at LNGS of a 50 litres prototype (PHASE_0) foreseen for last quarter of 2021 will be followed by a $O(1)$ m³ experiment (PHASE_1). While PHASE_0 will allow to

validate MC simulation and test CYGNO approaches performances in a underground environment, PHASE_1 will serve as test of the minimisation of the background of internal materials radioactivity and of the scalability to larger volume. From the results of these phases, a large scale experiment ($30\text{-}100 \text{ m}^3$) will be proposed, to explore the 1-10 GeV WIMP mass region with high sensitivity to both SI and SD coupling and directionality. A preliminary sensitivity reach to WIMP searches was hence evaluated for PHASE_2 with different background assumptions, reflecting realistic scenarios of performance improvements.
805 This study demonstrates that PHASE_2 would bring a significant contribution to WIMP searches, not only by probing parameters space unexplored to these days, but also being the only approach able to confirm and study any future DM claim by other experiments in this region, for both SI and SD couplings. Additional compelling physics cases accessible thanks to experiment directional capabilities have been discussed, for
810 which detailed studies are being carried out.

The CYGNO approach results therefore highly promising and is expected to be able to significantly contribute to the advancement of TPC technology in the rare event search field.

7. *Acknowledgements

820 Appendix A Statistical analysis for the sensitivity limit evaluation

The estimation of the expected limits of the CYGNO experiment was performed applying a Bayesian based method. In principle, this approach allows to calculate the probability of any model, given a certain amount of information (data) related to it. This methodology is rarely used in this field, even though it is recently gaining ground [96–103].

Every model, parameter which is of interest to the specific analysis, and experimental data are all considered connected to a probability distribution and, as such, follow the rules of probability. Exploiting the Bayes' theorem it is possible to find a relation between them and infer a final probability, called posterior, for the desired quantity. In the case of the CYGNO experiment one is interested in knowing, given a certain number of observed events per year, the probability that some of them are produced by a DM-nucleus interactions. Those can be events of background (μ_b) or of signal (μ_s), which is strictly connected to the cross section of WIMP DM particle with protons. The Bayes' theorem can be expressed as follows:

$$p(\mu, \theta | D, H) = \frac{p(D|\mu, \theta, H)\pi(\mu, \theta|H)}{\int_{\Omega} \int_0^{\infty} p(D|\mu, \theta, H)\pi(\mu, \theta|H)d\mu d\theta} \quad (A1)$$

with $p(D|\mu_s, \theta, H)$ representing the likelihood function $L(\mu_s, \theta)$.

In equation eq. A1, the following notation is used:

- $p(\mu|D)$, posterior probability function for the parameter μ , given D .
- $\pi(\mu)$, prior probability of a parameter. It includes the expectations of the parameters as well as constraints and knowledge previously obtained from other experiments.
- μ , free and of interest parameter representing the expected events due to WIMP-induced recoil (μ_s) or background (μ_b), given a certain WIMP mass (the analysis performs a raster scan).
- θ , vector of nuisance parameters, necessary to describe theoretical assumptions and experimental conditions that can affect the results. They can be not completely known and may depend on prior probability distributions. For example, when $\mu = \mu_s, \mu_b$, the events expected from the background, becomes a nuisance parameter.
- D , data set. Can be made of actual experimental data or simulated ones.
- H , hypothesis under test. It can be the hypothesis of pure background, H_0 , or the one where both background and signal are present, H_1 .
- Ω , nuisance parameters space.

The likelihood function used to obtain the results shown in Sec.5.1 is defined as:

$$p(D|\mu_s, \mu_b, H_1) = (\mu_b + \mu_s)^{N_{evt}} e^{-(\mu_b + \mu_s)} \prod_{i=1}^{N_{bins}} \left[\left(\frac{\mu_b}{\mu_b + \mu_s} P_{i,b} + \frac{\mu_s}{\mu_b + \mu_s} P_{i,s} \right)^{n_i} \frac{1}{n_i!} \right] \quad (A2)$$

with:

- N_{evt} , total number of events of the data sample.
- i , index representing the bin of the histogram in the 2D angular Galactic coordinates.
- n_i , number of events occurring in the i -th bin.
- μ , the expected events due to WIMP-induced recoil (μ_s) or background (μ_b), given a certain WIMP mass.
- $P_{i,x}$, Probability of single event to end up in the i -th bin, according to x model (background or signal).

The $P_{i,x}$ marginalized probability includes the effects due to the theoretical angular distribution, the migration from one bin to another caused by resolution effects, and which element recoils. Being in the context of estimating the limits of the CYGNO experiment when data result consistent with a pure background hypothesis, once the

posterior probability of the parameter μ_s is evaluated, it is possible to compute the upper bound as the 90% Credible Interval (C.I.). This is defined as follows:

$$\mu_s(90\%CI) : \int_0^{\mu_s(90\%CI)} p(\mu_s | \mathcal{D}, H_1) d\mu_s = 0.9 \quad (\text{A3})$$

where $p(\mu_s | \mathcal{D}, H_1)$ is the posterior probability marginalised over the nuisance parameters. This value represents the limit under which the true value of μ_s is, with a 90% of probability.

References

1. Bertone, G.; Hooper, D.; Silk, J. Particle dark matter: Evidence, candidates and constraints. *Phys. Rept.* **2005**, *405*, 279–390, [[hep-ph/0404175](#)]. doi:10.1016/j.physrep.2004.08.031.
2. Mayet, F.; others. A review of the discovery reach of directional Dark Matter detection. *Phys. Rept.* **2016**, *627*, 1–49, [[arXiv:astro-ph.CO/1602.03781](#)]. doi:10.1016/j.physrep.2016.02.007.
3. Zurek, K.M. Asymmetric Dark Matter: Theories, Signatures, and Constraints. *Phys. Rept.* **2014**, *537*, 91–121, [[arXiv:hep-ph/1308.0338](#)]. doi:10.1016/j.physrep.2013.12.001.
4. Petraki, K.; Volkas, R.R. Review of asymmetric dark matter. *Int. J. Mod. Phys. A* **2013**, *28*, 1330028, [[arXiv:hep-ph/1305.4939](#)]. doi:10.1142/S0217751X13300287.
5. Hochberg, Y.; Kuflik, E.; Murayama, H.; Volansky, T.; Wacker, J.G. Model for Thermal Relic Dark Matter of Strongly Interacting Massive Particles. *Phys. Rev. Lett.* **2015**, *115*, 021301, [[arXiv:hep-ph/1411.3727](#)]. doi:10.1103/PhysRevLett.115.021301.
6. Essig, R.; Mardon, J.; Volansky, T. Direct Detection of Sub-GeV Dark Matter. *Phys. Rev. D* **2012**, *85*, 076007, [[arXiv:hep-ph/1108.5383](#)]. doi:10.1103/PhysRevD.85.076007.
7. Essig, R.; Manalaysay, A.; Mardon, J.; Sorensen, P.; Volansky, T. First Direct Detection Limits on sub-GeV Dark Matter from XENON10. *Phys. Rev. Lett.* **2012**, *109*, 021301, [[arXiv:astro-ph.CO/1206.2644](#)]. doi:10.1103/PhysRevLett.109.021301.
8. Agnes, P.; others. Constraints on Sub-GeV Dark-Matter-Electron Scattering from the DarkSide-50 Experiment. *Phys. Rev. Lett.* **2018**, *121*, 111303, [[arXiv:astro-ph.CO/1802.06998](#)]. doi:10.1103/PhysRevLett.121.111303.
9. Crisler, M.; Essig, R.; Estrada, J.; Fernandez, G.; Tiffenberg, J.; Sofo haro, M.; Volansky, T.; Yu, T.T. SENSEI: First Direct-Detection Constraints on sub-GeV Dark Matter from a Surface Run. *Phys. Rev. Lett.* **2018**, *121*, 061803, [[arXiv:hep-ex/1804.00088](#)]. doi:10.1103/PhysRevLett.121.061803.
10. Agnese, R.; others. First Dark Matter Constraints from a SuperCDMS Single-Charge Sensitive Detector. *Phys. Rev. Lett.* **2018**, *121*, 051301, [[arXiv:hep-ex/1804.10697](#)]. [Erratum: *Phys. Rev. Lett.* **2019**, *122*, 069901 (2019)], doi:10.1103/PhysRevLett.121.051301.
11. Aprile, E.; others. Excess electronic recoil events in XENON1T. *Phys. Rev. D* **2020**, *102*, 072004, [[arXiv:hep-ex/2006.09721](#)]. doi:10.1103/PhysRevD.102.072004.
12. Bernabei, R.; others. On electromagnetic contributions in WIMP quests. *Int. J. Mod. Phys. A* **2007**, *22*, 3155–3168, [[arXiv:astro-ph/0706.1421](#)]. doi:10.1142/S0217751X07037093.
13. Ibe, M.; Nakano, W.; Shoji, Y.; Suzuki, K. Migdal Effect in Dark Matter Direct Detection Experiments. *JHEP* **2018**, *03*, 194, [[arXiv:hep-ph/1707.07258](#)]. doi:10.1007/JHEP03(2018)194.
14. Bell, N.F.; Dent, J.B.; Newstead, J.L.; Sabharwal, S.; Weiler, T.J. Migdal effect and photon bremsstrahlung in effective field theories of dark matter direct detection and coherent elastic neutrino-nucleus scattering. *Phys. Rev. D* **2020**, *101*, 015012, [[arXiv:hep-ph/1905.00046](#)]. doi:10.1103/PhysRevD.101.015012.
15. Dolan, M.J.; Kahlhoefer, F.; McCabe, C. Directly detecting sub-GeV dark matter with electrons from nuclear scattering. *Phys. Rev. Lett.* **2018**, *121*, 101801, [[arXiv:hep-ph/1711.09906](#)]. doi:10.1103/PhysRevLett.121.101801.
16. Baracchini, E.; Derocco, W.; Dho, G. Discovering supernova-produced dark matter with directional detectors. *Phys. Rev. D* **2020**, *102*, 075036, [[arXiv:hep-ph/2009.08836](#)]. doi:10.1103/PhysRevD.102.075036.
17. Seguinot, J.; Ypsilantis, T.; Zichichi, A. A High rate solar neutrino detector with energy determination. *Conf. Proc. C* **1992**, *920310*, 289–313.

- 895 18. Arpesella, C.; Broggini, C.; Cattadori, C. A possible gas for solar neutrino spectroscopy. *Astropart. Phys.* **1996**, *4*, 333–341. doi:10.1016/0927-6505(95)00051-8.
- 896 19. Vahsen, S.E.; others. CYGNUS: Feasibility of a nuclear recoil observatory with directional sensitivity to dark matter and neutrinos **2020**. [[arXiv:physics.ins-det/2008.12587](#)].
- 900 20. Marx, J.N.; Nygren, D.R. The Time Projection Chamber. *Phys. Today* **1978**, *31N10*, 46–53. doi:10.1063/1.2994775.
- 905 21. Nygren, D.R. The Time Projection Chamber: A New 4 pi Detector for Charged Particles. *eConf* **1974**, *C740805*, 58.
- 910 22. Atwood, W.B.; others. Performance of the ALEPH time projection chamber. *Nucl. Instrum. Meth. A* **1991**, *306*, 446–458. doi:10.1016/0168-9002(91)90038-R.
- 915 23. Alme, J.; others. The ALICE TPC, a large 3-dimensional tracking device with fast readout for ultra-high multiplicity events. *Nucl. Instrum. Meth. A* **2010**, *622*, 316–367, [[arXiv:physics.ins-det/1001.1950](#)]. doi:10.1016/j.nima.2010.04.042.
- 920 24. Lippmann, C. Upgrade of the ALICE Time Projection Chamber **2014**.
- 925 25. Chardonnet, E. The DUNE dual-phase liquid argon TPC. *JINST* **2020**, *15*, C05064. doi:10.1088/1748-0221/15/05/C05064.
- 930 26. Fraga, M.M.F.R.; Fraga, F.A.F.; Fetal, S.T.G.; Margato, L.M.S.; Ferreira-Marques, R.; Policarpo, A.J.P.L. The GEM scintillation in He CF₄, Ar CF₄, Ar TEA and Xe TEA mixtures. *Nucl. Instrum. Meth.* **2003**, *A504*, 88–92. doi:10.1016/S0168-9002(03)00758-7.
- 935 27. Margato, L.M.S.; Morozov, A.; Fraga, M.M.F.R.; Pereira, L.; Fraga, F.A.F. Effective decay time of CF₄ secondary scintillation. *JINST* **2013**, *8*, P07008. doi:10.1088/1748-0221/8/07/P07008.
- 940 28. Baracchini, E.; Benussi, L.; Bianco, S.; Capoccia, C.; Caponero, M.; Cavoto, G.; Cortez, A.; Costa, I.A.; Marco, E.D.; D'Imperio, G.; Dho, G.; Iacoangeli, F.; Maccarrone, G.; Marafini, M.; Mazzitelli, G.; Messina, A.; Orlandi, A.; Paoletti, E.; Passamonti, L.; Petrucci, F.; Piccolo, D.; Pierluigi, D.; Pinci, D.; Renga, F.; Rosatelli, F.; Russo, A.; Saviano, G.; Tomassini, S. First evidence of luminescence in a He/CF₄ gas mixture induced by non-ionizing electrons, **2020**, [[arXiv:physics.ins-det/2004.10493](#)].
- 945 29. Monteiro, C.M.B.; Fernandes, L.M.P.; Veloso, J.F.C.A.; Oliveira, C.A.B.; dos Santos, J.M.F. Secondary scintillation yield from GEM and THGEM gaseous electron multipliers for direct dark matter search. *Phys. Lett. B* **2012**, *714*, 18–23. doi:10.1016/j.physletb.2012.06.066.
- 950 30. Dominik, W.; Zaganidis, N.; Astier, P.; Charpak, G.; Santiard, J.C.; Sauli, F.; Tribollet, E.; Geissbuhler, A.; Townsend, D. A GASEOUS DETECTOR FOR HIGH ACCURACY AUTORADIOGRAPHY OF RADIOACTIVE COMPOUNDS WITH OPTICAL READOUT OF AVALANCHE POSITIONS. *Nucl. Instrum. Meth. A* **1989**, *278*, 779. doi:10.1016/0168-9002(89)91203-5.
- 955 31. Sauli, F. GEM: A new concept for electron amplification in gas detectors. *Nucl. Instrum. Meth. A* **1997**, *386*, 531–534. doi:10.1016/S0168-9002(96)01172-2.
- 960 32. Margato, L.M.S.; Fraga, F.A.F.; Fetal, S.T.G.; Fraga, M.M.F.R.; Balau, E.F.S.; Blanco, A.; Ferreira-Marques, R.; Policarpo, A.J.P.L. Performance of an optical readout GEM-based TPC. *Nucl. Instrum. Meth.* **2004**, *A535*, 231–235. doi:10.1016/j.nima.2004.07.126.
- 965 33. Marafini, M.; Patera, V.; Pinci, D.; Sarti, A.; Sciubba, A.; Spiriti, E. High granularity tracker based on a Triple-GEM optically read by a CMOS-based camera. *JINST* **2015**, *10*, P12010, [[arXiv:physics.ins-det/1508.07143](#)]. doi:10.1088/1748-0221/10/12/P12010.
- 970 34. Phan, N.S.; Lee, E.R.; Loomba, D. Imaging ⁵⁵Fe Electron Tracks in a GEM-based TPC Using a CCD Readout. *arXiv* **1703.09883** **2017**, [[arXiv:physics.ins-det/1703.09883](#)].
- 975 35. Fraga, F.A.F.; Margato, L.M.S.; Fetal, S.T.; Fraga, M.M.F.R.; Ferreira-Marques, R.; Policarpo, A.J.P.L.; Guerard, B.; Oed, A.; Manzini, G.; van Vuure, T. CCD readout of GEM-based neutron detectors. *Nucl. Instrum. Meth. A* **2002**, *478*, 357–361. doi:10.1016/S0168-9002(01)01829-0.
- 980 36. Mavrokordidis, K.; Ball, F.; Carroll, J.; Lazos, M.; McCormick, K.J.; Smith, N.A.; Touramanis, C.; Walker, J. Optical Readout of a Two Phase Liquid Argon TPC using CCD Camera and THGEMs. *JINST* **2014**, *9*, P02006, [[arXiv:physics.ins-det/1401.0525](#)]. doi:10.1088/1748-0221/9/02/P02006.
- 985 37. Marafini, M.; Patera, V.; Pinci, D.; Sarti, A.; Sciubba, A.; Spiriti, E. ORANGE: A high sensitivity particle tracker based on optically read out GEM. *Nucl. Instrum. Meth.* **2017**, *A845*, 285–288. doi:10.1016/j.nima.2016.04.014.
- 990 38. Antochi, V.C.; Baracchini, E.; Cavoto, G.; Marco, E.D.; Marafini, M.; Mazzitelli, G.; Pinci, D.; Renga, F.; Tomassini, S.; Voena, C. Combined readout of a triple-GEM detector. *JINST* **2018**, *13*, P05001, [[arXiv:physics.ins-det/1803.06860](#)]. doi:10.1088/1748-0221/13/05/P05001.

- 955 39. Marafini, M.; Patera, V.; Pinci, D.; Sarti, A.; Sciubba, A.; Torchia, N.M. Study of the Performance of an Optically Readout Triple-GEM. *IEEE Transactions on Nuclear Science* **2018**, *65*, 604–608. doi:10.1109/TNS.2017.2778503.
- 960 40. Pinci, D.; Baracchini, E.; Cavoto, G.; Marco, E.D.; Marafini, M.; Mazzitelli, G.; Renga, F.; Tomassini, S.; Voena, C. High resolution TPC based on optically readout GEM. *Nuclear Instruments and Methods in Physics Research Section A: Accelerators, Spectrometers, Detectors and Associated Equipment* **2018**. doi:<https://doi.org/10.1016/j.nima.2018.11.085>.
- 965 41. Antochi, V.C.; Cavoto, G.; Costa, I.A.; Marco, E.D.; D'Imperio, G.; Iacoangeli, F.; Marafini, M.; Messina, A.; Pinci, D.; Renga, F.; Voena, C.; Baracchini, E.; Cortez, A.; Dho, G.; Benussi, L.; Bianco, S.; Capoccia, C.; Caponero, M.; Maccarrone, G.; Mazzitelli, G.; Orlandi, A.; Paoletti, E.; Passamonti, L.; Piccolo, D.; Pierluigi, D.; Rosatelli, F.; Russo, A.; Saviano, G.; Tomassini, S.; Nobrega, R.A.; Petrucci, F. A GEM-based Optically Readout Time Projection Chamber for charged particle tracking, 2020, [[arXiv:physics.ins-det/2005.12272](https://arxiv.org/abs/physics.ins-det/2005.12272)].
- 970 42. Costa, I.A.; Baracchini, E.; Bellini, F.; Benussi, L.; Bianco, S.; Caponero, M.; Cavoto, G.; D'Imperio, G.; Marco, E.D.; Maccarrone, G.; Marafini, M.; Mazzitelli, G.; Messina, A.; Petrucci, F.; Piccolo, D.; Pinci, D.; Renga, F.; Rosatelli, F.; Saviano, G.; Tomassini, S. Stability and detection performance of a GEM-based Optical Readout TPC with He/CF₄ gas mixtures. *Journal of Instrumentation* **2020**, *xx*, xxx. doi:yy.y.
- 975 43. Campagnola, R. Study and optimization of the light-yield of a triple-GEM detector **2018**.
44. Veenhof, R. Garfield, a drift chamber simulation program. *Conf. Proc. C* **1993**, *9306149*, 66–71.
45. Veenhof, R. GARFIELD, recent developments. *Nucl. Instrum. Meth. A* **1998**, *419*, 726–730. doi:10.1016/S0168-9002(98)00851-1.
- 980 46. Agostinelli, S.; others. GEANT4: A Simulation toolkit. *Nucl. Instrum. Meth. A* **2003**, *506*, 250–303. doi:10.1016/S0168-9002(03)01368-8.
47. Costa, I.A.; Baracchini, E.; Bellini, F.; Benussi, L.; Bianco, S.; Caponero, M.; Cavoto, G.; D'Imperio, G.; Marco, E.D.; Maccarrone, G.; Marafini, M.; Mazzitelli, G.; Messina, A.; Petrucci, F.; Piccolo, D.; Pinci, D.; Renga, F.; Rosatelli, F.; Saviano, G.; Tomassini, S. Performance of optically readout GEM-based TPC with a 55Fe source. *Journal of Instrumentation* **2019**, *14*, P07011–P07011. doi:10.1088/1748-0221/14/07/p07011.
- 985 48. Antochi, V.; Baracchini, E.; Benussi, L.; Bianco, S.; Capoccia, C.; Caponero, M.; Cavoto, G.; Cortez, A.; Costa, I.; Di Marco, E.; et al.. Performance of an optically read out time projection chamber with ultra-relativistic electrons. *Nuclear Instruments and Methods in Physics Research Section A: Accelerators, Spectrometers, Detectors and Associated Equipment* **2021**, *999*, 165209, [[arXiv:physics.ins-det/2005.12272v3](https://arxiv.org/abs/physics.ins-det/2005.12272v3)]. doi:10.1016/j.nima.2021.165209.
49. B.Buonomo.; C.Di Giulio.; L.G.Foggetta.; P.Valente. A Hardware and Software Overview on the New BTF Transverse Profile Monitor. Proc. 5th Int. Beam Instrumentation Conf. (IBIC'16), Barcelona, Spain, 2016, pp. 818–821. doi:10.18429/JACoW-IBIC2016-WE PG73.
- 990 50. P.Valente.; B.Buonomo.; Di Giulio, C.; L.G.Foggetta. Frascati Beam-Test Facility (BTF) High Resolution Beam Spot Diagnostics. Proc. 5th Int. Beam Instrumentation Conf. (IBIC'16), Barcelona, Spain, 2016, pp. 222–225. doi:10.18429/JACoW-IBIC2016-MOPG65.
51. Blum, W.; Rolandi, L.; Riegler, W. *Particle detection with drift chambers; Particle Acceleration and Detection*, ISBN = 9783540766834, 2008. doi:10.1007/978-3-540-76684-1.
- 995 52. Pinci, D. A triple-GEM detector for the muon system of the LHCb experiment. PhD thesis, Cagliari University, CERN-THESIS-2006-070, 2006.
53. Baracchini, E.; others. A density-based clustering algorithm for the CYGNO data analysis. *JINST* **2020**, *15*, T12003, [[arXiv:physics.ins-det/2007.01763](https://arxiv.org/abs/physics.ins-det/2007.01763)]. doi:10.1088/1748-0221/15/12/T12003.
- 1000 54. Ester, M.; Kriegel, H.P.; Sander, J.; Xu, X. A Density-based Algorithm for Discovering Clusters a Density-based Algorithm for Discovering Clusters in Large Spatial Databases with Noise. Proceedings of the Second International Conference on Knowledge Discovery and Data Mining. AAAI Press, 1996, KDD'96, pp. 226–231.
55. Caselles, V.; Kimmel, R.; Sapiro, G. Geodesic Active Contours. *International Journal of Computer Vision* **1997**, *22*, 61–79.
- 1005 56. P. Marquez-Neila and L. Baumela and L. Alvarez. A Morphological Approach to Curvature-Based Evolution of Curves and Surfaces. *IEEE Transactions on Pattern Analysis and Machine Intelligence* **2014**, *36*, 2–17.
57. Baracchini, E.; others. Identification of low energy nuclear recoils in a gas TPC with optical readout **2020**. [[arXiv:physics.ins-det/2007.12508](https://arxiv.org/abs/physics.ins-det/2007.12508)]. doi:10.1088/1361-6501/abbd12.

58. Daw, E.; others. The DRIFT Directional Dark Matter Experiments. *EAS Publ. Ser.* **2012**, *53*, 11–18, [[arXiv:physics.ins-det/1110.0222](#)]. doi:10.1051/eas/1253002.
59. Battat, J.B.R.; others. Low Threshold Results and Limits from the DRIFT Directional Dark Matter Detector. *Astropart. Phys.* **2017**, *91*, 65–74, [[arXiv:astro-ph.IM/1701.00171](#)]. doi:10.1016/j.astropartphys.2017.03.007.
- 1015 60. Battat, J.B.R.; others. Reducing DRIFT Backgrounds with a Submicron Aluminized-Mylar Cathode. *Nucl. Instrum. Meth. A* **2015**, *794*, 33–46, [[arXiv:physics.ins-det/1502.03535](#)]. doi:10.1016/j.nima.2015.04.070.
61. Akl, M.A.; others. CMS Technical Design Report for the Muon Endcap GEM Upgrade **2015**.
- 1020 62. Riffard, Q.; others. MIMAC low energy electron-recoil discrimination measured with fast neutrons. *JINST* **2016**, *11*, P08011, [[arXiv:astro-ph.IM/1602.01738](#)]. doi:10.1088/1748-0221/11/08/P08011.
63. Phan, N.S.; Lauer, R.J.; Lee, E.R.; Loomba, D.; Matthews, J.A.J.; Miller, E.H. GEM-based TPC with CCD Imaging for Directional Dark Matter Detection. *Astropart. Phys.* **2016**, *84*, 82–96, [[arXiv:physics.ins-det/1510.02170](#)]. doi:10.1016/j.astropartphys.2016.08.006.
- 1025 64. Castel, J.; others. Background assessment for the TREX Dark Matter experiment. *Eur. Phys. J. C* **2019**, *79*, 782, [[arXiv:astro-ph.IM/1812.04519](#)]. doi:10.1140/epjc/s10052-019-7282-6.
65. Martoff, C.J.; Snowden-Ifft, D.P.; Ohnuki, T.; Spooner, N.; Lehner, M. Suppressing drift chamber diffusion without magnetic field. *Nucl. Instrum. Meth. A* **2000**, *440*, 355–359. doi:10.1016/S0168-9002(99)00955-9.
- 1030 66. Ohnuki, T.; Snowden-Ifft, D.P.; Martoff, C.J. Measurement of carbon disulfide anion diffusion in a TPC. *Nucl. Instrum. Meth. A* **2001**, *463*, 142–148, [[physics/0004006](#)]. doi:10.1016/S0168-9002(01)00222-4.
67. Battat, J.B.R.; others. Low Threshold Results and Limits from the DRIFT Directional Dark Matter Detector. *Astropart. Phys.* **2017**, *91*, 65–74, [[arXiv:astro-ph.IM/1701.00171](#)]. doi:10.1016/j.astropartphys.2017.03.007.
- 1035 68. Phan, N.S.; Lafler, R.; Lauer, R.J.; Lee, E.R.; Loomba, D.; Matthews, J.A.J.; Miller, E.H. The novel properties of SF₆ for directional dark matter experiments. *JINST* **2017**, *12*, P02012, [[arXiv:physics.ins-det/1609.05249](#)]. doi:10.1088/1748-0221/12/02/P02012.
69. Ikeda, T.; Shimada, T.; Ishiura, H.; Nakamura, K.D.; Nakamura, T.; Miuchi, K. Development of a negative ion micro TPC detector with SF₆ gas for the directional dark matter search. *JINST* **2020**, *15*, P07015, [[arXiv:physics.ins-det/2004.09706](#)]. doi:10.1088/1748-0221/15/07/P07015.
- 1040 70. Lightfoot, P.K.; Spooner, N.J.C.; Lawson, T.B.; Aune, S.; Giomataris, I. First operation of bulk micromegas in low pressure negative ion drift gas mixtures for dark matter searches. *Astropart. Phys.* **2007**, *27*, 490–499. doi:10.1016/j.astropartphys.2007.02.003.
71. Baracchini, E.; Cavoto, G.; Mazzitelli, G.; Murtas, F.; Renga, F.; Tomassini, S. Negative Ion Time Projection Chamber operation with SF₆ at nearly atmospheric pressure. *JINST* **2018**, *13*, P04022, [[arXiv:physics.ins-det/1710.01994](#)]. doi:10.1088/1748-0221/13/04/P04022.
- 1045 72. Lewin, J.; Smith, P. Review of mathematics, numerical factors, and corrections for dark matter experiments based on elastic nuclear recoil. *Astroparticle Physics* **1996**, *6*, 87–112. doi:[https://doi.org/10.1016/S0927-6505\(96\)00047-3](https://doi.org/10.1016/S0927-6505(96)00047-3).
73. Gondolo, P. Recoil momentum spectrum in directional dark matter detectors. *Physical Review D* **2002**, *66*, [[arXiv:hep-ph/0209110v2](#)]. doi:10.1103/physrevd.66.103513.
- 1050 74. Baxter, D.; Bloch, I.M.; Bodnia, E.; Chen, X.; Conrad, J.; Gangi, P.D.; Dobson, J.E.Y.; Durnford, D.; Haselschwardt, S.J.; Kaboth, A.; Lang, R.F.; Lin, Q.; Lippincott, W.H.; Liu, J.; Manalaysay, A.; McCabe, C.; Mora, K.D.; Naim, D.; Neilson, R.; Olcina, I.; Piro, M.C.; Selvi, M.; von Krosigk, B.; Westerdale, S.; Yang, Y.; Zhou, N. Recommended conventions for reporting results from direct dark matter searches, 2021, [[arXiv:hep-ex/2105.00599v1](#)].
- 1055 75. Nakamura, K.; others. Low pressure gas study for a direction-sensitive dark matter search experiment with MPGD. *JINST* **2012**, *7*, C02023. doi:10.1088/1748-0221/7/02/C02023.
76. Smith, M.C.; Ruchti, G.R.; Helmi, A.; Wyse, R.F.G.; Fulbright, J.P.; Freeman, K.C.; Navarro, J.F.; Seabroke, G.M.; Steinmetz, M.; Williams, M.; et al.. The RAVE survey: constraining the local Galactic escape speed. *Monthly Notices of the Royal Astronomical Society* **2007**, *379*, 755–772. doi:10.1111/j.1365-2966.2007.11964.x.
- 1060 77. Aprile, E.; Aalbers, J.; Agostini, F.; Alfonsi, M.; Althueser, L.; Amaro, F.; Anthony, M.; Arneodo, F.; Baudis, L.; Bauermeister, B.; et al.. Dark Matter Search Results from a One Ton-Year Exposure of XENON1T. *Physical Review Letters* **2018**, *121*, [[arXiv:astro-ph.CO/1805.12562v2](#)]. doi:10.1103/physrevlett.121.111302.

- 1070 78. Aprile, E.; Aalbers, J.; Agostini, F.; Alfonsi, M.; Althueser, L.; Amaro, F.; Antochi, V.; Angelino, E.; Arneodo, F.; Barge, D.; et al.. Light Dark Matter Search with Ionization Signals in XENON1T. *Physical Review Letters* **2019**, *123*, [[arXiv:hep-ex/1907.11485v2](#)]. doi:10.1103/physrevlett.123.251801.
- 1075 79. Boehm, C.; Cerdeño, D.; Machado, P.; Campo, A.O.D.; Reid, E. How high is the neutrino floor? *Journal of Cosmology and Astroparticle Physics* **2019**, *2019*, 043–043, [[arXiv:hep-ph/1809.06385v4](#)]. doi:10.1088/1475-7516/2019/01/043.
- 1080 80. Agnes, P.; Albuquerque, I.; Alexander, T.; Alton, A.; Araujo, G.; Asner, D.; Ave, M.; Back, H.; Baldin, B.; Batignani, G.; et al.. Low-Mass Dark Matter Search with the DarkSide-50 Experiment. *Physical Review Letters* **2018**, *121*, [[arXiv:astro-ph.HE/1802.06994v3](#)]. doi:10.1103/physrevlett.121.081307.
- 1085 81. Agnese, R.; Anderson, A.; Aralis, T.; Aramaki, T.; Arnquist, I.; Baker, W.; Balakishiyeva, D.; Barker, D.; Basu Thakur, R.; Bauer, D.; et al.. Low-mass dark matter search with CDMSlite. *Physical Review D* **2018**, *97*, [[arXiv:astro-ph.CO/1707.01632v3](#)]. doi:10.1103/physrevd.97.022002.
- 1090 82. Mancuso, M.; others. Searches for Light Dark Matter with the CRESST-III Experiment. *J. Low Temp. Phys.* **2020**, *199*, 547–555. doi:10.1007/s10909-020-02343-3.
- 1095 83. Savage, C.; Gelmini, G.; Gondolo, P.; Freese, K. Compatibility of DAMA/LIBRA dark matter detection with other searches. *Journal of Cosmology and Astroparticle Physics* **2009**, *2009*, 010–010, [[arXiv:astro-ph/0808.3607v3](#)]. doi:10.1088/1475-7516/2009/04/010.
- 1100 84. Agnese, R.; others. Projected Sensitivity of the SuperCDMS SNOLAB experiment. *Phys. Rev. D* **2017**, *95*, 082002, [[arXiv:physics.ins-det/1610.00006](#)]. doi:10.1103/PhysRevD.95.082002.
- 1105 85. Willers, M.; others. Direct dark matter search with the CRESST-III experiment - status and perspectives. *J. Phys. Conf. Ser.* **2017**, *888*, 012209. doi:10.1088/1742-6596/888/1/012209.
- 1110 86. Aalseth, C.E.; others. Future Dark Matter Searches with Low-Radioactivity Argon, by The Global Argon Dark Matter Collaboration. *Input to the European Particle Physics Strategy Update*.
- 1115 87. Savage, C.; Gondolo, P.; Freese, K. Can WIMP spin dependent couplings explain DAMA data, in light of null results from other experiments? *Physical Review D* **2004**, *70*, [[arXiv:astro-ph/0408346v3](#)]. doi:10.1103/physrevd.70.123513.
- 1120 88. Battat, J.; Ezeribe, A.; Gauvreau, J.L.; Harton, J.; Lafler, R.; Law, E.; Lee, E.; Loomba, D.; Lumnah, A.; Miller, E.; et al.. Low threshold results and limits from the DRIFT directional dark matter detector. *Astroparticle Physics* **2017**, *91*, 65–74, [[arXiv:astro-ph.IM/1701.00171v3](#)]. doi:10.1016/j.astropartphys.2017.03.007.
- 1125 89. Amole, C.; Ardid, M.; Arnquist, I.; Asner, D.; Baxter, D.; Behnke, E.; Bressler, M.; Broerman, B.; Cao, G.; Chen, C.; et al.. Dark matter search results from the complete exposure of the PICO-60 C3F8 bubble chamber. *Physical Review D* **2019**, *100*, [[arXiv:astro-ph.CO/1902.04031v1](#)]. doi:10.1103/physrevd.100.022001.
- 1130 90. Yakabe, R.; Nakamura, K.; Ikeda, T.; Ito, H.; Yamaguchi, Y.; Taishaku, R.; Nakazawa, M.; Ishiura, H.; Nakamura, T.; Shimada, T.; Tanimori, T.; Kubo, H.; Takada, A.; Sekiya, H.; Takeda, A.; Miuchi, K. First limits from a 3d-vector directional dark matter search with the NEWAGE-0.3b' detector, 2020, [[arXiv:hep-ex/2005.05157](#)].
- 1135 91. DeRocco, W.; Graham, P.W.; Kasen, D.; Marques-Tavares, G.; Rajendran, S. Supernova signals of light dark matter. *Phys. Rev. D* **2019**, *100*, 075018, [[arXiv:hep-ph/1905.09284](#)]. doi:10.1103/PhysRevD.100.075018.
- 1140 92. Billard, J.; Strigari, L.; Figueroa-Feliciano, E. Implication of neutrino backgrounds on the reach of next generation dark matter direct detection experiments. *Phys. Rev. D* **2014**, *89*, 023524, [[arXiv:hep-ph/1307.5458](#)]. doi:10.1103/PhysRevD.89.023524.
- 1145 93. Boehm, C.; Cerdeño, D.G.; Machado, P.A.N.; Olivares-Del Campo, A.; Perdomo, E.; Reid, E. How high is the neutrino floor? *JCAP* **2019**, *01*, 043, [[arXiv:hep-ph/1809.06385](#)]. doi:10.1088/1475-7516/2019/01/043.
- 1150 94. Bertuzzo, E.; Deppisch, F.F.; Kulkarni, S.; Perez Gonzalez, Y.F.; Zukanovich Funchal, R. Dark Matter and Exotic Neutrino Interactions in Direct Detection Searches. *JHEP* **2017**, *04*, 073, [[arXiv:hep-ph/1701.07443](#)]. doi:10.1007/JHEP04(2017)073.
- 1155 95. Soffitta, P.; Mulieri, F.; Fabiani, S.; Costa, E.; Bellazzini, R.; Brez, A.; Minuti, M.; Pinchera, M.; Spandre, G. Measurement of the position resolution of the Gas Pixel Detector. *Nucl. Instrum. Meth. A* **2013**, *700*, 99–105, [[arXiv:astro-ph.IM/1208.6330](#)]. doi:10.1016/j.nima.2012.09.055.

96. Roszkowski, L.; Ruiz de Austri, R.; Silk, J.; Trotta, R. On prospects for dark matter indirect detection in the Constrained MSSM. *Physics Letters B* **2009**, *671*, 10–14, [[\[0707.0622v2\]](#)]. doi: <https://doi.org/10.1016/j.physletb.2008.11.061>.
- 1130 97. Trotta, R.; de Austri, R.R.; Roszkowski, L. Prospects for direct dark matter detection in the constrained MSSM. *New Astronomy Reviews* **2007**, *51*, 316–320, [[\[arXiv:astro-ph/0609126v1\]](#)]. Francesco Melchiorri: Scientist, Pioneer, Mentor, doi:<https://doi.org/10.1016/j.newar.2006.11.059>.
- 1135 98. Sturge, C.; Trotta, R.; Bertone, G.; Peter, A.H.G.; Scott, P. Fundamental statistical limitations of future dark matter direct detection experiments. *Physical Review D* **2012**, *86*, [[\[arXiv:hep-ph/1201.3631v2\]](#)]. doi:10.1103/physrevd.86.023507.
- 1140 99. Arina, C. Bayesian analysis of multiple direct detection experiments, 2014, [[\[arXiv:hep-ph/1310.5718\]](#)].
100. Bringmann, T.; Conrad, J.; Cornell, J.M.; Dal, L.A.; Edsjö, J.; Farmer, B.; Kahlhoefer, F.; Kvellestad, A.; Putze, A.; et al.. DarkBit: a GAMBIT module for computing dark matter observables and likelihoods. *The European Physical Journal C* **2017**, *77*, [[\[arXiv:hep-ph/1705.07920v2\]](#)]. doi:10.1140/epjc/s10052-017-5155-4.
- 1145 101. Liem, S.; Bertone, G.; Calore, F.; de Austri, R.R.; Tait, T.M.P.; Trotta, R.; Weniger, C. Effective field theory of dark matter: a global analysis. *Journal of High Energy Physics* **2016**, *2016*, [[\[arXiv:hep-ph/1603.05994v1\]](#)]. doi:10.1007/jhep09(2016)077.
102. Messina, A.; Nardecchia, M.; Piacentini, S. Annual modulations from secular variations: not relaxing DAMA? *Journal of Cosmology and Astroparticle Physics* **2020**, *2020*, 037–037, [[\[arXiv:hep-ph/2003.03340v2\]](#)]. doi:10.1088/1475-7516/2020/04/037.
- 1150 103. di Cortona, G.G.; Messina, A.; Piacentini, S. Migdal effect and photon Bremsstrahlung: improving the sensitivity to light dark matter of liquid argon experiments. *Journal of High Energy Physics* **2020**, *2020*, [[\[arXiv:hep-ph/2006.02453v2\]](#)]. doi:10.1007/jhep11(2020)034.

